The local hole revealed by galaxy counts and redshifts

J. R. Whitbourn★ and T. Shanks★

Extragalactic & Cosmology Group, Department of Physics, Durham University, South Road DH1 3LE, UK

ABSTRACT

The redshifts of $\approx250\,000$ galaxies are used to study the local hole and its associated peculiar velocities. The sample, compiled from the 6dF Galaxy Redshift Survey and Sloan Digital Sky Survey, provides wide sky coverage to a depth of $\approx300\,h^{-1}$ Mpc. We have therefore examined K- and r-limited galaxy redshift distributions and number counts to map the local density field. Comparing observed galaxy $n(z)$ distributions to homogeneous models in three large regions of the high-latitude sky, we find evidence for underdensities ranging from $\approx$4–40 per cent in these regions to depths of $\approx150\,h^{-1}$ Mpc with the deepest underdensity being over the southern Galactic cap. Using the Galaxy and Mass Assembly survey, we then establish the normalization of galaxy counts at fainter magnitudes and thus confirm that the underdensity over all three fields at $K < 12.5$ is $\approx15 \pm 3$ per cent. Finally, we further use redshift catalogues to map sky-averaged peculiar velocities over the same areas using the average redshift–magnitude, $\bar{z}(m)$, technique of Soneira. After accounting for the direct effect of the large-scale structure on $\bar{z}(m)$, we can then search for peculiar velocities. Taking all three regions into consideration, the data reject at the $\approx4\sigma$ level the idea that we have recovered the cosmic microwave background rest frame in the volume probed. We therefore conclude that there is some consistent evidence from both counts and Hubble diagrams for a 'local hole' with an $\approx150\,h^{-1}$ Mpc underdensity that deeper counts and redshifts in the northern Galactic cap suggest may extend to $\approx300\,h^{-1}$ Mpc.

Key words: methods: analytical – galaxies: general – Local Group – large-scale structure of Universe – infrared: galaxies.

1 INTRODUCTION

The cosmological principle is a fundamental assumption of cosmology that leads us to describe our universe as statistically homogeneous and isotropic, which uniquely gives the Friedmann–Lemaître–Robertson–Walker solutions to Einstein's field equations. These metrics are apparently successful, encompassing many current observations of the Universe over huge scales in space, time and energy.

However, at least locally, the validity of the cosmological principle is less obvious. Deep redshift surveys such as Sloan Digital Sky Survey (SDSS; York et al. 2000) and Two-degree-Field Galaxy Redshift Survey (2dFGRS; Colless et al. 2001) have revealed a web-like structure to the galaxy distribution with extensive and ongoing clustering at knots and junctions. Indeed, recent redshift surveys have found this large-scale structure (LSS) persisting up to at least scales of $300\,h^{-1}$ Mpc (Gott et al. 2005; Murphy, Eke & Frenk 2011). The results are in concordance with Λ cold dark matter (ΛCDM) N-body simulations with the galaxies displaying the expected hierarchical structure from individual galaxies to galaxy clusters to superclusters (Park et al. 2012; Watson et al. 2013). The visible structures are

parsed by large coherent regions of underdensity known as voids, which can be of $\mathcal{O}(50\,\mathrm{Mpc})$. Compared to galaxy clusters, voids were a relatively recent discovery in cosmography as they required large-redshift surveys to easily separate galaxies in the same line of sight by redshift. These regions seem to be approximately spherical and underdense in all types of matter (Rood 1988; Peebles & Nusser 2010).

The question of the local galaxy density has received renewed attention due to the challenges represented by the recent measurements of a Λ-like accelerated expansion of the universe (Schmidt et al. 1998; Perlmutter et al. 1999). There is the possibility that the role of Λ in producing the dimming of the $m - z$ relationship for SN1a could instead be due to the acceleration induced by a large local underdensity. Recently, it has been shown that $\mathcal{O}(\mathrm{Gpc})$ local hole models can accurately mimic Λ whilst accounting for independent scale factor measurements (February et al. 2010). However, it remains unclear as to whether these models can equally well simultaneously account for other cosmological data sets[1] – see Biswas, Notari & Valkenburg (2010), Moss, Zibin & Scott (2011) and also Nadathur & Sarkar (2011) and Regis & Clarkson (2012).

---

[1] Baryon acoustic oscillations, $H(z)$, Kinetic Sunyaev–Zel'dovich, lithium abundance, cosmic microwave background (CMB) fluctuations and cosmic shear.

★ E-mails: joseph.whitbourn@durham.ac.uk (JRW);
Tom.Shanks@durham.ac.uk (TS)

1.1 Scale of homogeneity

Results disagree as to whether recent redshift surveys have approached the depths required to describe the universe as statistically homogeneous. Studies of the fractal dimension of the galaxy distribution typically report a homogeneity scale of $\approx 70\,h^{-1}$ Mpc (Hogg et al. 2005; Sarkar et al. 2009; Scrimgeour et al. 2012). However, other studies instead find the presence of LSS beyond these scales and indeed persisting to the relevant survey depths (Célérier & Thieberger 2005; Labini 2011).

Efforts to use the number or flux dipole in a similar manner to the peculiar velocity dipole have been in concordance with the ΛCDM standard model (Blake & Wall 2002; Bilicki et al. 2011). Gibelyou & Huterer (2012) report that the NRAO VLA Sky Survey number dipole is unexpectedly large; however, they attribute this to potential systematic errors.

Studies of the structure of our local peculiar velocity field have used the scale at which the bulk peculiar velocity is that of the CMB dipole as a proxy for the scale of homogeneity. Some authors have reported a relatively local origin within $\approx 60\,h^{-1}$ Mpc for the dipole (Erdoğdu et al. 2006). However, other recent studies have suggested that there are bulk flows at much larger scales (Watkins, Feldman & Hudson 2009; Feldman, Watkins & Hudson 2010; Colin et al. 2011; Abate & Feldman 2012). These results are in contrast with a series of papers (Nusser, Branchini & Davis 2011; Branchini, Davis & Nusser 2012), where a method similar to one used here is pioneered and bulk flows consistent with ΛCDM were found.

Furthermore, attempts to infer the bulk velocity field with respect to the CMB have typically returned values incompatible with homogeneity (Kashlinsky et al. 2008; Lavaux, Afshordi & Hudson 2013). These results are however disputed by some authors (Keisler 2009; Osborne et al. 2011).

1.2 Number counts

By counting the number of galaxies as a function of magnitude and redshift, strong constraints can be imposed on galaxy evolution, galaxy distribution and cosmology. The existence of LSS in the form of superstructures such as filaments can be readily detected in these counts (Frith et al. 2003).

In the standard model with Λ, number counts for $z < 1$ are well described by simple pure luminosity evolution (PLE) models where galaxies form at high redshift and evolve according to their galaxy star formation rate (SFR), with e-folding times assumed to be $\tau = 1-2.5$ Gyr for redder types and $\tau = 9$ Gyr for bluer types. These PLE models are successful across a wide range of passbands and to considerable redshift depth (Shanks et al. 1984; Metcalfe et al. 2001, 2006; Hill et al. 2011).

However, the above PLE models cannot simultaneously account for bright and faint magnitude counts (Metcalfe et al. 2001; Liske et al. 2003). Specifically, the counts in the range $10 < B < 17$ mag are significantly steeper than expected from a non-evolving model. Indeed, the counts at fainter magnitudes are less steep relative to such a model. As long as the PLE model counts were normalized at $B \approx 18$ mag, the PLE models then fit in the range $18 < B < 28.5$ (Metcalfe et al. 2001) but attempts to fit at $B < 17$ inevitably overshoot beyond $B > 17$, and it seemed puzzling that the evolution rate should increase at lower redshift. It was therefore suggested that the steepness of the bright counts may be caused by a local underdensity (Shanks et al. 1984). Luminosity functions (LFs) measured in redshift surveys are reasonably consistent in form but there exists considerable variation in ϕ^* (Cross et al. 2001; Liske et al. 2003). This uncertainty is in part due to the failure of non-evolving (or sim-

ple PLE) models to fit bright and faint counts simultaneously and is known as the normalization problem. There is supporting evidence for a faint count normalization from several previous studies (Driver et al. 1995; Glazebrook et al. 1995), complemented by results from the latest and deepest number counts (Barro et al. 2009; Keenan et al. 2010) and LFs (Keenan et al. 2012; Keenan, Barger & Cowie 2013).

A further argument against the steep bright counts being caused by $z < 0.1$ galaxy evolution is that the steepness is observed across the NIR and optical bands (*B,R,I,H,K*) (Metcalfe et al. 2001, 2006). In models where the SFR dominates the evolution, we should expect the bluer bands to be more affected than the redder bands, and this effect is seen at fainter magnitudes but not at brighter magnitudes.

Using early (partial) Two Micron All-Sky Survey (2MASS) data releases, Frith embarked on a series of analyses at bright NIR magnitudes to investigate the strong local LSS hypothesis. Frith et al. (2003) observed evidence for the reality of the proposed local underdensity with the underdensities in the 2dFGRS redshift distribution accounting well for the underdense 2MASS number counts – see also Busswell et al. (2004). The galaxy distribution was found to be patchy with large regions of under- and overdensity. Across the whole sky a coherent ≈ 15–20 per cent underdensity, a local hole, on the scale of $\mathcal{O}(300\,\text{Mpc})$ was consistent with these data.

Frith, Metcalfe & Shanks (2006) also found further evidence that the faint normalization is correct in the *H* band. Using a set of 2MASS mocks, the full sky underdensity was found to represent a 2.5σ fluctuation for a ΛCDM model.

In this paper, we attempt to extend the Frith, Shanks & Outram (2005b) analysis of the local hole hypothesis. We first check out the connection between $n(z)$ and $n(m)$ in substantially bigger areas than available to Frith et al. We also test whether there is an underdensity in the mass as well as the galaxy counts by estimating a velocity field using the Metcalfe et al. (2001) LF and the $\bar{z}(m)$ Hubble diagram technique of Soneira (1979) which we outline below.

2 TECHNIQUES

2.1 Number–magnitude and number–redshift distributions

We will first compare the number–redshift and number–magnitude distributions with those that assume homogeneous models. We assume simple LFs as described by Metcalfe et al. (2001) and so predict the differential number redshift relation $n(z)$ using

$$n(z)\,\mathrm{d}z = 4\pi r(z)^2 \frac{\mathrm{d}r}{\mathrm{d}z}\mathrm{d}z \int_{-\infty}^{M(m_{\mathrm{lim}},z)} \Phi(M)\,\mathrm{d}M, \tag{1}$$

where m_{lim} is the survey magnitude limit, $r(z)$ is the comoving radial coordinate, $\Phi(M)$ is the differential Schechter (1976) LF in comoving units with characteristic absolute magnitude and density, $M^*(z)$ and $\phi^*(z)$ and slope α. Our models for the redshift dependence of $M^*(z)$ include K- plus E-corrections from Bruzual & Charlot (2003) models with ϕ^* and α held constant for individual galaxy types for the homogeneous models. We shall generally normalize the homogeneous $n(z)$ model to exceed the observed $n(z)$ by the ratio of homogeneous model counts to the observed $n(m)$. We shall then simply divide the observed $n(z)$ by the homogeneous model $n(z)$ to determine how the galaxy density $\phi^*(z)$ varies with redshift.

The homogeneous number–magnitude relation is then similarly calculated as

$$n(m)\Delta m = \int_0^\infty 4\pi r(z)^2 \frac{\mathrm{d}r}{\mathrm{d}z}\mathrm{d}z \int_{M(m_b,z)}^{M(m_f,z)} \Phi(M)\,\mathrm{d}M, \tag{2}$$

where $m = (\frac{m_b + m_f}{2})$ and $\Delta m = m_f - m_b$. We can then also input $\phi^*(z)$ from $n(z)$ into the $n(m)$ model to check for consistency between any under- or overdensities found in $n(z)$ and $n(m)$.

2.2 Hubble diagrams from galaxy redshift surveys

Hubble's law relates cosmological redshifts to distance. Usually the distances come from standard candles or rods for individual galaxies. But here we aim to use the galaxy LF as the standard candle for magnitude-limited samples of galaxies using the average redshift as a function of magnitude, $\bar{z}(m)$, following Soneira (1979). In essence, the method assumes a universal LF which is an approximation, ignoring environmental effects. But the bigger the volumes averaged, the more this assumption will apply and the LF can then be used as a statistical standard candle.

Soneira (1979), working at small redshifts, assumed a Euclidean cosmology and the redshift–distance relation, $z = br^p + y$, where the peculiar velocity y distribution is described by $Q(y)$, and derived

$$\bar{z}(m) \propto 10^{0.2pm}. \tag{3}$$

Clearly for a linear Hubble law, $p = 1$ and the aim of Soneira's analysis was to determine p. Here we use the same technique out to higher redshift where the potential effects of cosmology, K-correction and evolution cannot be ignored. We can describe $\bar{z}(m)$ in complete generality using the volume element dV/dr, the differential LF $\Phi(M)$, the peculiar velocity distribution $Q(y)$ and K- plus E-corrections,

$$\bar{z}(m) = \frac{\int_{-\infty}^{\infty} dy \int_0^{\infty} z(r, y) Q(y) \Phi(m - 5 \log d_L - 25 - \mathrm{KE}(z)) \frac{dV}{dr} dr}{\int_{-\infty}^{\infty} dy \int_0^{\infty} Q(y) \Phi(m - 5 \log d_L - 25 - \mathrm{KE}(z)) \frac{dV}{dr} dr}.$$

We initially only make the simplest set of assumptions about $Q(y)$, that it is normalized to one and with a mean of zero, i.e. non-streaming,

$$\int_{-\infty}^{\infty} Q(y)\, dy = 1, \quad \int_{-\infty}^{\infty} y\, Q(y)\, dy = 0. \tag{4}$$

In the case of velocity flows, we have more complicated forms of $Q(y)$. The simplest such case is a bulk flow where all galaxies are moving coherently,

$$\int_{-\infty}^{\infty} y\, Q(y)\, dy = \frac{v_{\mathrm{flow}}}{c}. \tag{5}$$

The implication for $\bar{z}(m)$ is that

$$\bar{z}(m) = \bar{z}_{\mathrm{hubble}}(m) + \frac{v_{\mathrm{flow}}}{c}. \tag{6}$$

Therefore, $\bar{z}(m)$ is dependent on the galaxy streaming velocity.

$\bar{z}(m)$ is calculated in magnitude bins. We have chosen to use both $\delta m = 0.5$ and $\delta m = 0.1$. The larger $\delta m = 0.5$ binning is preferred because these have slightly smaller errors and reduced covariance between bins. However, we have also presented results for $\bar{z}(m)$ with the smaller magnitude binning size of $\delta m = 0.1$ to investigate the sensitivity of $\bar{z}(m)$ to individual elements of LSS, which the larger binning suppresses.

3 MODELLING

We now need to model $n(z)$, $n(m)$ and $\bar{z}(m)$ first in the homogeneous case so below we present details of the galaxy evolution models and the LF parameters.

Table 1. Parameters for the zero-redshift LF as assumed here (Metcalfe et al. 2001, 2006). We will use a ΛCDM cosmology with $\Omega_\Lambda = 0.7$, $\Omega_{\mathrm{m}} = 0.3$ and $h = 0.7$.

Type	$\phi\ (h^3\ \mathrm{Mpc}^{-3})$	α	$M_{\mathrm{R}}^* - 5\log(h)$	$R - K$
E/S0	7.416×10^{-3}	-0.7	-20.93	2.48
Sab	3.704×10^{-3}	-0.7	-20.75	2.52
Sbc	4.960×10^{-3}	-1.1	-20.87	2.45
Scd	2.184×10^{-3}	-1.5	-20.70	2.13
Sdm	1.088×10^{-3}	-1.5	-20.62	1.58

3.1 Galaxy evolution models

A galaxy's apparent magnitude is dependent on both evolution and SED; hence, modelling $\bar{z}(m)$ requires us to account for the $k(z)$ and $e(z)$ effects. The K- plus E-corrections used in this paper are calculated using the stellar synthesis models set out in Bruzual & Charlot (2003). We have used an $x = 3$ IMF for early types to mimic the PLE galaxy models set out by Metcalfe et al. (2001, 2006).

In this paper, we will usually present results in the NIR and at low redshift, where the $e(z)$- and $k(z)$-corrections are relatively small and can be reasonably well determined. This is because the NIR is dominated by old stars and hence is insensitive to different star formation histories (Cole et al. 2001; Bruzual & Charlot 2003). We have verified this by experimenting with alternative forms for the $k(z)$- and $e(z)$-correction and found that the results are not sensitive to the exact form used.

3.2 Luminosity functions

Our basic LF will be taken from Metcalfe et al. (2001). This is a type-dependent LF that is inferred from the optical and translated into the NIR using the mean colours (see Table 1). Modelling of the number counts, redshift distributions and $\bar{z}(m)$ using this LF has been done using the full number count programme described by Metcalfe et al. (1996).

3.3 Radial inhomogeneity – LSS correction

The derivation of $\bar{z}(m)$ shown earlier assumes radial homogeneity $\bar{z}(\bar{r}) = \bar{z}(r)$ which leads to a sensitivity to over/underdensities, as was indeed originally noted by Soneira (1979). For example, the presence of a local hole would be expected to cause a boost to $\bar{z}(m)$ at bright magnitudes (small distances), even with no induced peculiar motion. This is because at a bright apparent magnitude, m, the ratio of galaxies outside the hole (with high z) to galaxies inside the hole (at low z) would be expected to increase with hole density contrast and scale. The inverse would be expected in the presence of a local overdensity.

We can model this effect by varying the normalization ϕ^* of the LF we use. To do this, we will include radial density profiles derived from our $n(z)$ distributions. Rather than allowing this measure to extend to the survey limits where the effect of redshift incompleteness and survey systematics becomes more prominent, we set a scale z_{global} where we transition to the expected homogeneous value. We use values of $z_{\mathrm{global}} = 0.15$ and 0.25 for the K and r bands, respectively,

$$\phi^*(z) = \begin{cases} \frac{n(z)_{\mathrm{obs}}}{n(z)_{\mathrm{model}}} \phi^*_{\mathrm{global}} & \text{if } z \leq z_{\mathrm{global}} \\ \phi^*_{\mathrm{global}} & \text{if } z > z_{\mathrm{global}}. \end{cases} \tag{7}$$

We assume that the density variations in the $n(z)$ are real and use this to correct the $\bar{z}(m)$ model prediction for the effect of LSS

before looking for residuals that can be interpreted as peculiar velocities v_{pec}. We shall also use the same technique to correct our homogeneous model $n(m)$ prediction for the effect of LSS to make consistency checks between $n(m)$ and $n(z)$.

In a following paper, Shanks & Whitbourn (in preparation) will use simple maximum likelihood (ML) estimates of the LF also to estimate $\phi^*(z)$ simultaneously. We find that the Metcalfe et al. (2001) LF used here is in good agreement with these ML estimates. The $\phi^*(z)$ density runs with redshift also agree with those reported below.

3.4 Error calculation

As a first approximation, it is possible to assume Poisson errors for the number counts and standard errors for $\overline{z}(m)$. This though is unrealistic for real galaxy distributions since galaxies cluster. To account for this, we have therefore calculated jack-knife errors. These were calculated using $10° \times 10°$ sub-fields. For N fields denoted by k, the errors on a statistic f as a function of the variable x are

$$\sigma_f^2(x) = \frac{N-1}{N} \sum_k^N (f_k(x) - \overline{f}(x))^2, \tag{8}$$

where $f_k(x)$ is the average of the fields excluding field k. We have experimented with both more survey-specific sub-fields and alternative methods such as field-to-field resampling and find approximately equivalent results in these cases.

4 DATA – SURVEYS

In this section, a compilation is given of the key characteristics of the imaging and redshift surveys used throughout this work. We shall generally use pseudo-total magnitudes, usually estimated by integrating a fitted analytic surface brightness profile to large radii – for details see individual surveys below. We shall use magnitudes zero-pointed in the Vega system throughout. This is primarily for ease since the 2MASS photometry is quoted in this system. Where necessary we have converted from AB to Vega using the following offsets from Hill et al. (2011) and Blanton & Roweis (2007),

$$K_{\mathrm{vega}} = K_{\mathrm{AB}} - 1.90,$$

$$r_{\mathrm{vega}} = r_{\mathrm{AB}} - 0.16. \tag{9}$$

The NIR is minimally affected by dust extinction but we have applied extinction corrections using the extinction maps of Schlegel, Finkbeiner & Davis (1998). We note that our results are insensitive to whether we apply the correction at all. This applies in r as well as K since the r band data used below are restricted to higher galactic latitudes.

In terms of the redshift surveys, we choose to work in the Local Group rest frame. All redshifts have therefore been corrected to the Local Group barycentre using $(l_{\mathrm{LG}}, b_{\mathrm{LG}}) = (93°, -4°)$ and $v_{\mathrm{LG}} = 316\,\mathrm{km\,s^{-1}}$ (Karachentsev & Makarov 1996),

$$cz_{\mathrm{LG}} = cz_\odot + v_{\mathrm{LG}}[\sin(b)\sin(b_{\mathrm{LG}})$$
$$+ \cos(b)\cos(b_{\mathrm{LG}})\cos(l - l_{\mathrm{LG}})]. \tag{10}$$

4.1 Imaging surveys

We next discuss the main characteristics of the imaging surveys used in this work. The details of the tests we have done on the magnitude scales, star–galaxy separation, etc. are given in Appendix A.

4.1.1 2MASS

The 2MASS (Skrutskie et al. 2006) is a photometric survey in the NIR (J, H, K_s). The final eXtended Source Catalogue (2MASS-XSC) comprises 1647 459 galaxies over approximately the whole sky (99.998 per cent sky coverage), with a photometric calibration varying by as little as 2–3 per cent (Jarrett et al. 2003). 2MASS is currently thought to be magnitude complete to $K < 13.5$ (Bell et al. 2003; Chodorowski et al. 2008).

The 2MASS-XSC data used in this paper come from the 'All-Sky Data Release' at the Infrared Processing and Analysis Center (IPAC) server. Galaxies have been included according to the following quality tags: '$cc\_flg = 0$', '$cc\_flg = Z$' to avoid contamination or confusion. The XSC catalogue consists solely of 2MASS objects with e-score and g-score <1.4 to ensure that the object really is extended and extragalactic.

It has been reported that the completeness and photometry of 2MASS-XSC galaxies with angular diameter greater than 10 arcmin may be affected by the limit on the 2MASS scan size (Jarrett et al. 2003). We have therefore applied a bright magnitude cut of $K > 10$ for $n(m)$, $n(z)$ and $\overline{z}(m)$.

For the 2MASS, we shall use a corrected form (see Appendix A) of their extrapolated isophotal, k_m_ext, magnitude. This total-type magnitude is based on an integration over the radial surface brightness profile. The lower radial boundary is defined by the isophotal $\mu = 20$ mag arcsec^{-2} radius and an upper boundary by four disc scalelengths unless that is greater than five of the above minimum isophotal radii.

4.1.2 GAMA

The Galaxy And Mass Assembly (GAMA; Driver et al. 2009) survey includes galaxies selected from UKIRT Infrared Deep Sky Survey – Large Area Survey (UKIDSS-LAS) and SDSS photometric targeting. It aims to create a catalogue of $\approx 350\,000$ galaxies with comprehensive photometry from the UV band to the radio. GAMA DR1 is based on three 45 deg^2 equatorial regions, chosen for their overlap with SDSS (stripes 9–12) and UKIDSS-LAS data. It comprises self-consistent ($ugrizJHK$) imaging of 114 441 galaxies with 50 282 science quality redshifts.

As of GAMA DR1, only the Kron-type K magnitude K_KRON has been provided, and therefore we use this magnitude type. Whilst the NIR GAMA photometric data come from UKIDSS, the final catalogue has been re-reduced for a variety of reasons outlined by Hill et al. (2011).

The GAMA data used here come from the DR1 release, GAMA-CoreDR1, described by Driver et al. (2011) and archived at http://www.gama-survey.org/database/YR1public.php. We have selected all galaxies in GAMA DR1, including those based on band-specific detections.

4.1.3 SDSS

The SDSS (York et al. 2000) covers ≈ 8500 deg^2 of the northern sky in the u, g, r, i, z bands. As of DR9 the survey comprises 208 478 448 galaxies and is magnitude complete to $r_{\mathrm{petro}} < 22.04$.

For consistency, we have chosen to work with the same magnitude type for both spectroscopic and photometric SDSS samples. We therefore use the 'cmodel'-type magnitude as recommended by SDSS.[2] This total-type magnitude is estimated by determining de

---

[2] https://www.sdss3.org/dr8/algorithms/magnitudes.php#which _mags

Vaucouleurs or exponential profiles for each object in each band. The likelihood of either profile is then determined, and the linear combination that best fits is then used to infer the total flux. A photometric sample has been selected using the quality criteria developed by Yasuda et al. (2001) for galaxy number counts. Namely, we reject saturated and non-primary objects and require a photometric classification as a galaxy in at least two of the g, r, i bands.

4.2 Redshift surveys

Next we describe the main characteristics of the redshift surveys used in this work. In Appendix B, we discuss the tests we have made on the magnitude-dependent spectroscopic incompleteness of these surveys and how such effects can be corrected in the redshift distributions, $n(z)$.

4.2.1 6dFGS

The 6dF Galaxy Redshift Survey (6dFGS; Jones et al. 2004) is a redshift survey over $\approx 17\,000$ deg^2, i.e. most of the southern sky, excluding $|b| < 10$. The survey was based on pre-existing overlapping survey photometry and was primarily selected in 2MASS K. The full survey comprises a catalogue of 125 071 galaxies with reliable redshifts. The survey has a median redshift of $z_{\text{median}} = 0.053$ (Jones et al. 2009) to its nominal limit of $K \leq 12.65$. We, however, shall be conservative and impose a $K < 12.5$ magnitude cut to minimize any completeness issues with the 6dFGS data. The 6dFGS data used in this paper come from the final DR3 release described in Jones et al. (2009) and is archived at http://www-wfau.roe.ac.uk/6dFGS/. Galaxies have been included according to the following quality tags: *quality* ≥ 3, *quality* $\neq 6$.

It is historically relevant to note that the 6dFGS survey was started before the final 2MASS photometry was released. Intermediate 2MASS photometry at low galactic latitudes was relatively shallow and suffered from poor spatial resolution. To work around this, the 6dFGS team adopted a pseudo-total magnitude for redshift targeting. Other researchers used an alternative $J - K$ inferred isophotal magnitude, hence referred to as a Cole type (Cole et al. 2001). With this type of estimator the less noisy J band is used to approach the true K-band magnitude as $K_{\text{cole}} = J_{\text{ext}} - (J_{\text{iso}} - K_{\text{iso}})$. This type was indeed found to have greater accuracy compared to the accurate photometry of Loveday (2000). However, the final release of the 2MASS catalogue provided the total estimator k_m_ext, as described earlier. The 6dFGS team recommend this magnitude

for science use. However, it remains the case that 6dFGS was targeted in a slightly different magnitude and that previous work has been conducted in a variety of magnitudes.

4.2.2 SDSS – spectroscopic survey

The spectroscopic sample was selected to a limit of $r_{\text{petro}} < 17.61$ finally comprising 1457 002 confirmed galaxy redshifts, with a median redshift $z_{\text{median}} = 0.108$. The SDSS spectroscopic sample was targeted on the basis of Petrosian magnitudes (Strauss et al. 2002). We however are working with the cmodel-type magnitude. To avoid selection and completeness effects, we therefore choose to work with the conservative magnitude limit $r_{\text{cmodel}} < 17.2$.

We have also created a K-limited SDSS spectroscopic sample by matching with 2MASS. The SDSS astrometric error is of the order of $\mathcal{O}(0.1 \text{ arcsec})$ (Finlator et al. 2000; Hill et al. 2011); we therefore set a 1 arcsec matching limit. For this K-limited SDSS sample, we are in effect applying the multiband selection that $K < 13.5$ and $r < 17.61$. This additional constraint does not bias the sample we select since even for a galaxy at the 2MASS limit it will require a relatively blue $r - K$ colour of 4.11 to avoid selection in the joint sample. Indeed, Bell et al. (2003) found that at most 1 per cent of galaxies were affected in a similar joint SDSS-2MASS sample.

The SDSS data used in this paper come from the DR9 main sample described in Ahn et al. (2012) and is archived at http://skyserver.sdss3.org/CasJobs/. In order to select a fair and high-quality sample of galaxies, we have used the following selection criteria: *class = 'GALAXY'*, ($zWarning = 0$ OR (($zWarning$&(4)) ≥ 0), *legacy_target*1&(64|128|256)) $\leq$ 0, *mode = 1* and *scienceprimary = 1*.

4.3 Target fields

Three fields were chosen to cover most of the northern and southern galactic caps at high latitudes while maintaining the basic division between the northern SDSS and southern 6dFGS redshift survey areas, as shown in Fig. 1 and Tables 2 and 3. The three fields are termed SDSS-NGC, 6dFGS-NGC and 6dFGS-SGC as shown in Fig. 1. These fields contain various regions of interest. The 6dFGS-NGC contains the CMB Local Group dipole pointing, the direction of Great Attractor and the Shapley-8 supercluster. The 6dFGS-SGC region contains the Perseus-Pisces supercluster, whilst the SDSS-NGC region contains the Coma cluster.
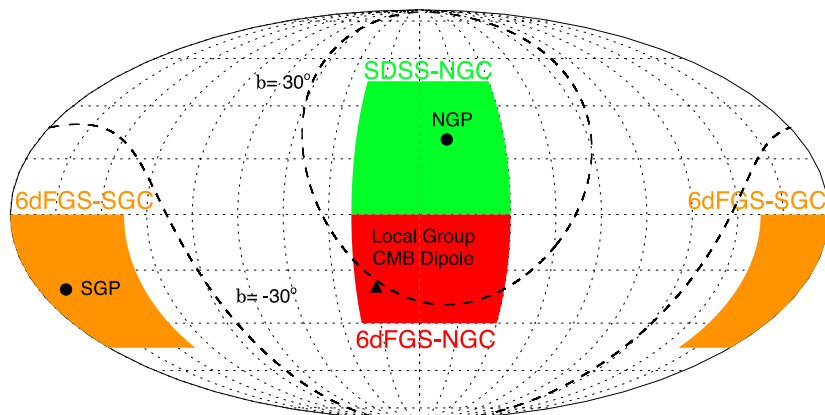

Figure 1. A Mollweide projection of the fields used in this study using the celestial coordinate system. The 6dFGS-NGC field is represented by the filled area in red, the 6dFGS-SGC field is shown by the filled area in orange and the SDSS-NGC is represented by the filled area in green. Also shown are the Northern and Southern Galactic Poles, the Local Group CMB dipole pointing and lines of $b = 30°$ and $b = -30°$ galactic latitude.

Table 2. A summary of the properties of the redshift and imaging surveys used; 6dFGS – Jones et al. (2004), SDSS – York et al. (2000), GAMA – Driver et al. (2009) and 2MASS – Jarrett et al. (2003).

Survey	z_{median}	Mag limit	Area (deg^2)
6dFGS	0.053	$K_s < 12.5$	17 000
SDSS-MAIN	0.108	$r < 17.61$	8500
GAMA	0.18	$r < 19.24$	150
2MASS	–	$K_s < 13.5$	∼ Full sky
SDSS-MAIN	–	$r < 22.04$	8500

Table 3. A summary of the main geometric properties of the target fields used.

Field	RA (J2000)	Dec. (J2000)	Area (deg^2)
6dFGS-NGC	[150, 220]	[−40, 0]	2578.03
6dFGS-SGC	[0–50, 330–360]	[−50, 0]	3511.29
SDSS-NGC	[150, 220]	[0, 50]	3072.38
GAMA G09	[129, 141]	[−1, 3]	47.98
GAMA G12	[174, 186]	[−2, 2]	47.99
GAMA G15	[211.5, 223.5]	[−2, 2]	47.99

5 REDSHIFT DISTRIBUTIONS

We first probe the local galaxy clustering environment directly via galaxy redshift distributions. Fig. 2 shows the $n(z)$ distributions consistently limited at $K < 12.5$ for our three target regions. Here we are using 2MASS magnitudes matched to 6dFGS redshifts in the case of 6dFGS-NGC and 6dFGS-SGC data and SDSS redshifts in the case of SDSS-NGC. Errors have been estimated from jack-knife errors within the three target regions. The red lines show the homogeneous $n(z)$ model estimated assuming the Metcalfe et al. (2001) LF and the K- plus E-corrections as outlined in Section 3. These models have been normalized so as to maintain the $K < 12.5$ $n(m)$ underdensities stated in Table 4 and corrected for redshift incompleteness (including any dependence of incompleteness on magnitude) using the method described in Appendix B.

We then divided the observed $n(z)$ by this suitably normalized homogeneous model to see over- and underdensities directly as a function of redshift. The results are shown in Fig. 3, and the significant non-uniformity we see reflects the presence of LSS in our local universe. With this $K < 12.5$ normalization, all three regions are typically underdense for $z < 0.05$ – see Table 4. The 6dFGS-SGC region, which corresponds to the Automatic Plate Measuring (APM) area (Maddox et al. 1990), is the most underdense at 40 ± 5 per cent. The error here comes from jack-knife estimates. The SDSS-NGC region is also significantly underdense at the 14 ± 5 per cent level. While the 6dFGS-NGC region still shows underdensity, it is not significantly so (4 ± 10 per cent). The error is bigger here because of the influence of the Shapley-8 supercluster in this region. Therefore, on scales out to $\approx 150\,h^{-1}$ Mpc, we conclude that the redshift distributions are consistently underdense by ≈ 4–40 per cent with the south Galactic cap showing the biggest underdensity.

Clearly a lot depends on the accuracy of the $n(K)$ model normalization. Frith et al. (2006) argued on the basis of a comparison of 2MASS $H < 12.5$ magnitude counts to much fainter counts from Calar Alto OmegaCAM that the Metcalfe et al. (2001) LF model normalization was supported by these data. However, this count was only based on an area of 0.25 deg^2. In Section 6.2, we shall test if

Table 4. A summary of the number count normalizations derived using the homogeneous Metcalfe et al. (2001) LF prediction. These also correspond to under- and overdensities to the specified limits. The $z < 0.05$ and $z < 0.1$ entries assume $K < 12.5$.

Field	Sample limit	Underdensity
6dFGS-NGC	$z < 0.05$	0.96 ± 0.10
6dFGS-SGC	$z < 0.05$	0.60 ± 0.05
SDSS-NGC	$z < 0.05$	0.86 ± 0.05
6dFGS-NGC	$z < 0.1$	0.94 ± 0.07
6dFGS-SGC	$z < 0.1$	0.75 ± 0.04
SDSS-NGC	$z < 0.1$	0.86 ± 0.04
6dFGS-NGC	$K < 12.5$	0.96 ± 0.07
6dFGS-SGC	$K < 12.5$	0.76 ± 0.03
SDSS-NGC	$K < 12.5$	0.88 ± 0.03
6dFGS-NGC	$K < 13.5$	1.03 ± 0.04
6dFGS-SGC	$K < 13.5$	0.92 ± 0.02
SDSS-NGC	$K < 13.5$	0.97 ± 0.02
SDSS-NGC	$r < 17.2$	0.96 ± 0.02

this normalization is consistent with the new K-band galaxy count data from the much bigger 150 deg^2 area of the GAMA survey.

It is also still possible that a larger scale underdensity persists beyond $z = 0.05$ out to $z \approx 0.1$. The underdensities then vary between 6 and 25 per cent as seen in Table 4. We find a weighted average underdensity of 15 ± 3 per cent for $K < 12.5$ (with or without a $z < 0.1$ cut). Certainly a similar conclusion was reached by Frith, Outram & Shanks (2005a) who had the advantage of the 2dFGRS $n(z)$ which reached fainter magnitudes and higher redshifts but only covering a significantly smaller region of sky. Again, the $n(z)$ model normalization is even more crucial in measuring any underdensity at $0.05 < z < 0.1$ because a lot depends on the position of the homogeneous model (red line) in Fig. 4. This can be probed both by galaxy counts to $K = 15.8$ in the 150 deg^2 GAMA regions and $n(z)$ to $K = 13.5$ by virtue of the deeper redshift survey data in the SDSS-NGC regions. But first we return to check that our $n(z)$ results are consistent with the *form* of the number counts to $K = 13.5$.

6 NUMBER COUNTS

6.1 2MASS galaxy counts to $K = 13.5$

Fig. 4 shows the number counts to $K < 13.5$ for our three regions. In Appendix A, we check for a scale error in the 2MASS magnitudes and the statistics of star–galaxy separation as a function of magnitude. In fact, we do find a marginal scale error within $10 < K < 13.5$, and all the magnitudes in Fig. 4 have been corrected for this scale error. With or without this correction, all fields exhibit an underdensity relative to the homogeneous prediction (red line) until at least $K \approx 12.5$ and any convergence is only seen when the counts reach $K = 13.5$. Using the $\phi^*(z)/\phi_{global}$ correction for radial inhomogeneity found earlier, we show the LSS-corrected model counts as the green line in Fig. 5 where observed counts have been normalized by the homogeneous model. We see that accounting for the inhomogeneities in the $n(z)$ in Fig. 3 has improved the model fit. This suggests a consistency between variations in the $n(z)$ and $n(m)$ and a mutual agreement in the redshift underdensity reported in Section 5.

These underdensities are either due to poor normalization of the models at fainter magnitudes, evolutionary brightening of
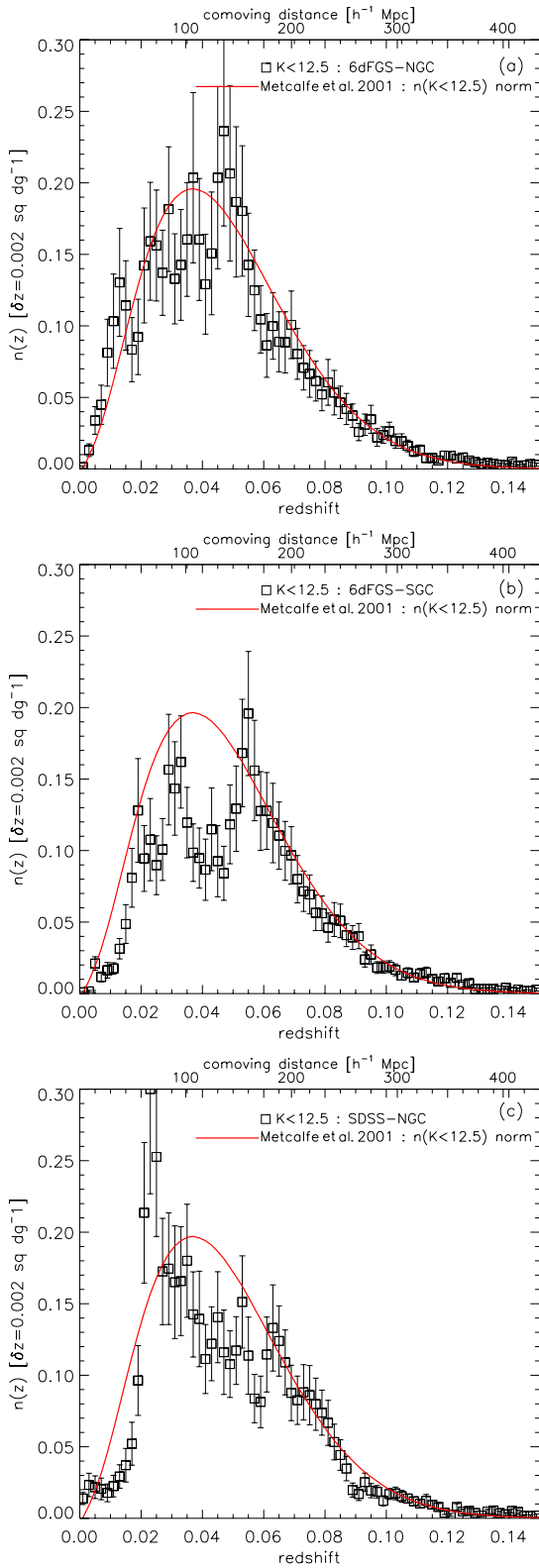
Figure 2. *K*-band galaxy *n*(*z*) with *K* < 12.5 and δ*z* = 0.002 normalized using the *K* < 12.5 galaxy number counts. The red line represents the homogeneous Metcalfe et al. (2001) LF prediction. The points (black square) show data with jack-knife derived errors. (a) 6dFGS-NGC region (6dFGS, galactic north), (b) 6dFGS-SGC region (6dFGS, galactic south), (c) SDSS-NGC (SDSS-2MASS, galactic north).
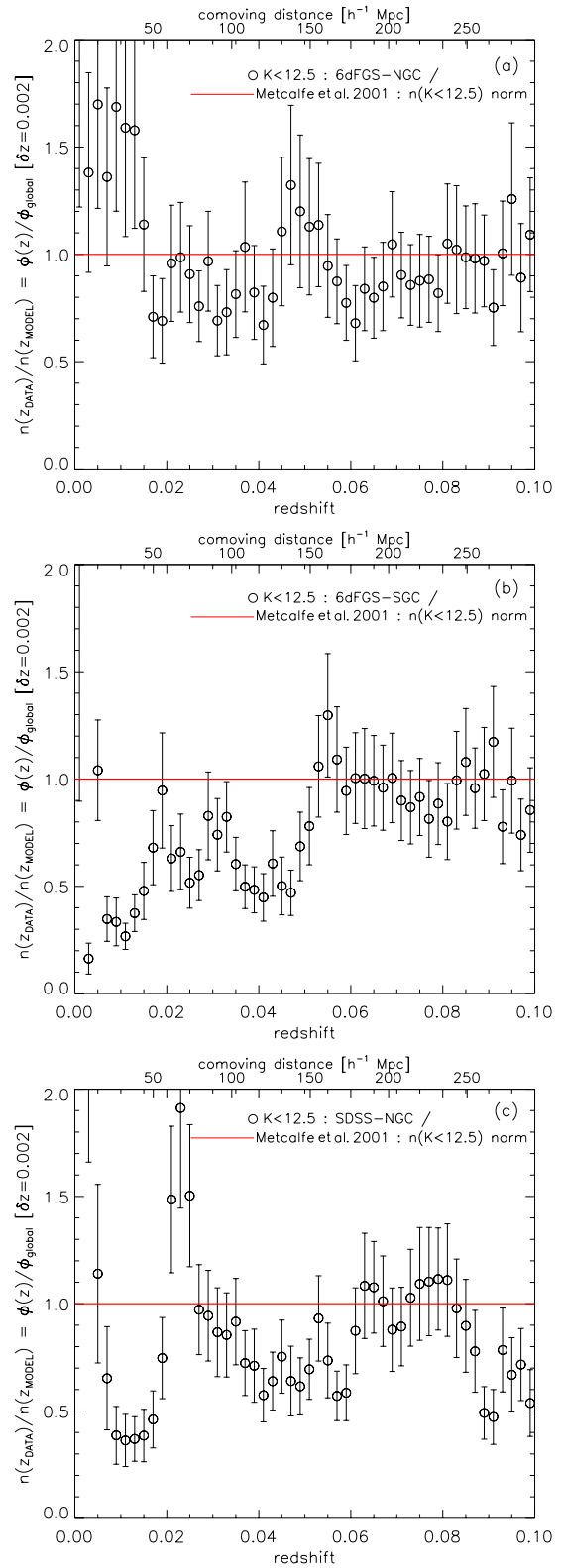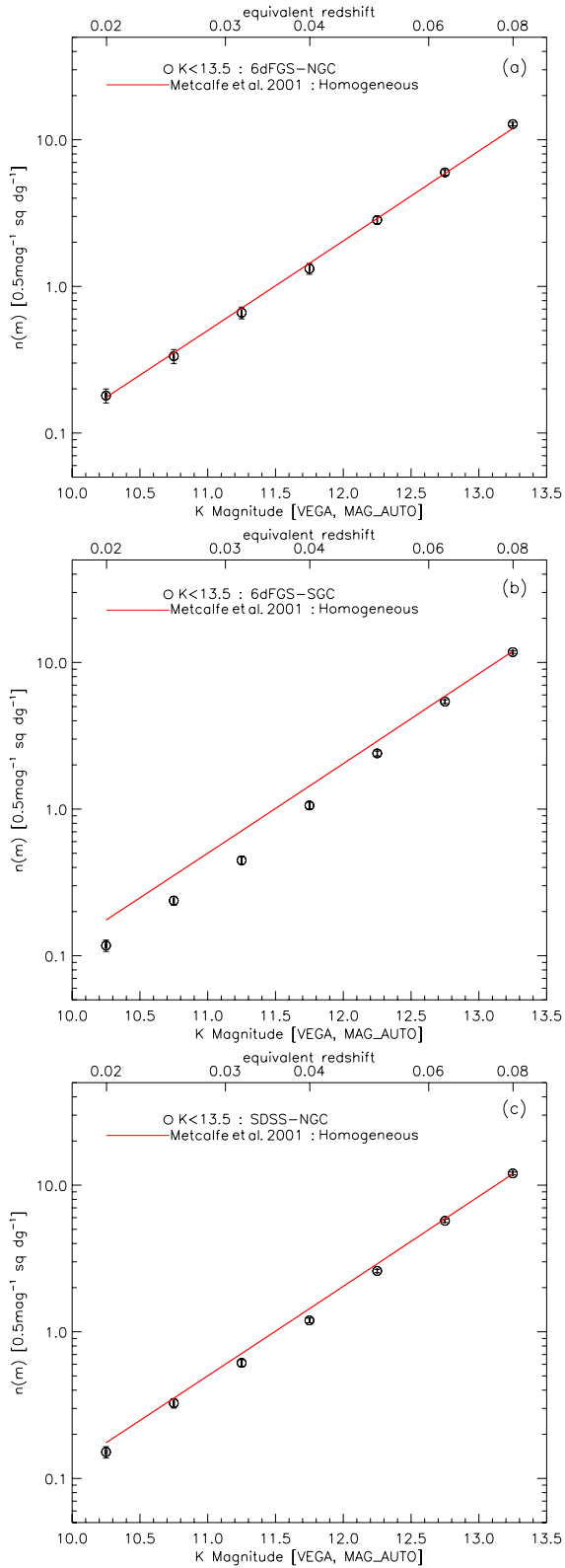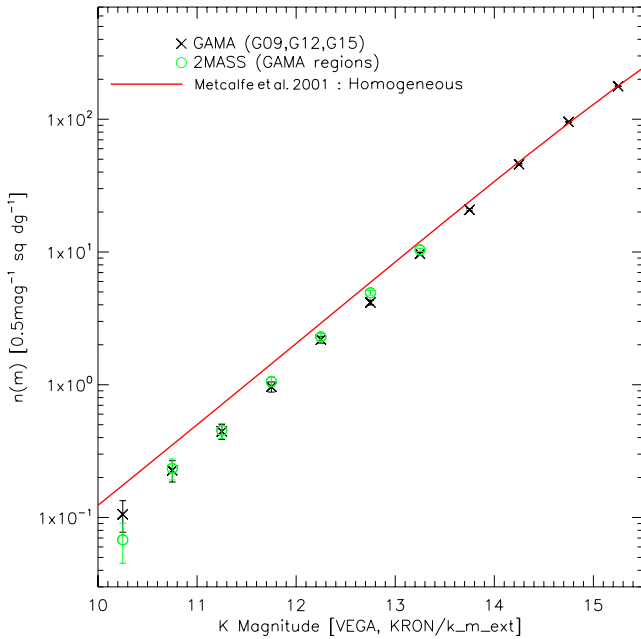
Figure 3. *K*-band galaxy φ*(*z*)/φ$_{global}$ with *K* < 12.5 and δ*z* = 0.002 normalized using the *K* < 12.5 galaxy number counts. The red line represents the homogeneous Metcalfe et al. (2001) LF prediction. The points (black circle) show data with jack-knife derived errors. (a) 6dFGS-NGC region (6dFGS, galactic north), (b) 6dFGS-SGC region (6dFGS, galactic south), (c) SDSS-NGC (SDSS-2MASS, galactic north).

Figure 4. *K*-band galaxy *n*(*m*) from the 2MASS with $\delta m = 0.5$. The red line represents the homogeneous Metcalfe et al. (2001) LF prediction. The points (black circle) show data with jack-knife derived errors. (a) 6dFGS-NGC region (6dFGS, galactic north), (b) 6dFGS-SGC region (6dFGS, galactic south), (c) SDSS-NGC (SDSS-2MASS, galactic north).
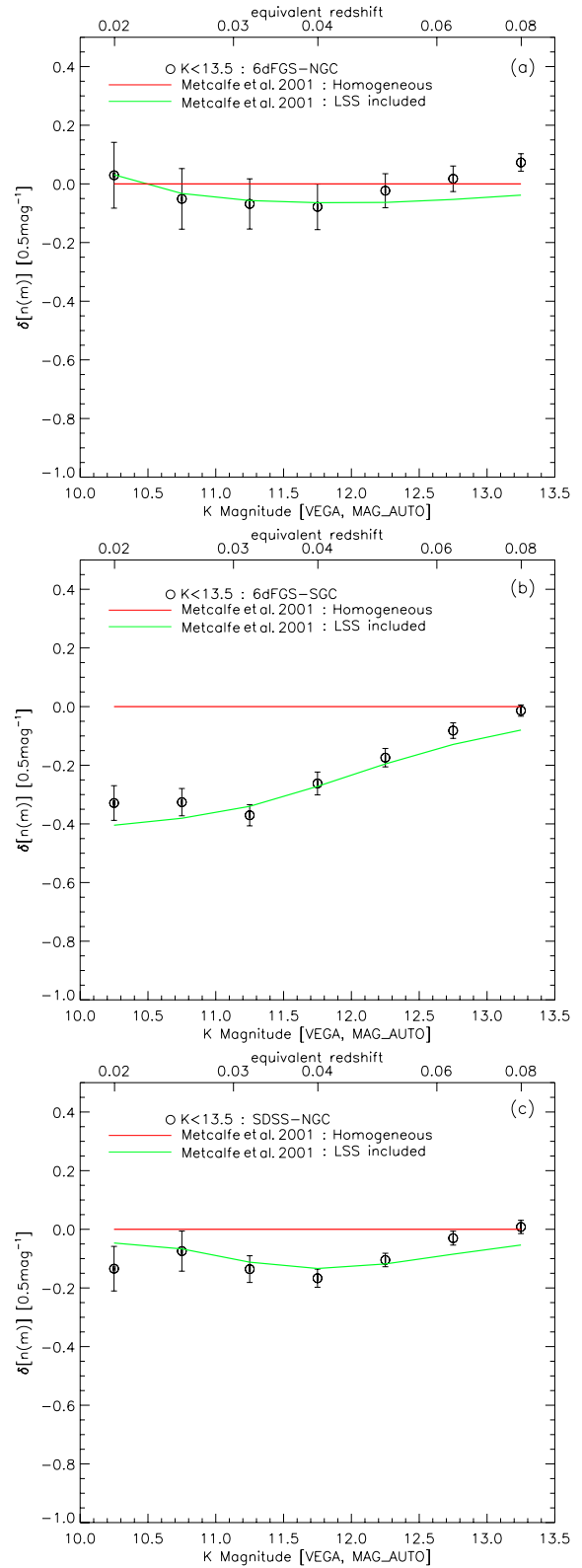
Figure 5. *K*-band galaxy *n*(*m*) density contrast from the 2MASS with $\delta m = 0.5$. The red line represents the homogeneous Metcalfe et al. (2001) LF prediction and the green line the LSS-corrected Metcalfe et al. (2001) LF prediction. The points (black circle) show data with jack-knife derived errors. (a) 6dFGS-NGC region (6dFGS, galactic north), (b) 6dFGS-SGC region (6dFGS, galactic south), (c) SDSS-NGC (SDSS-2MASS, galactic north).

Figure 6. *K*-band galaxy number counts comparing GAMA and 2MASS over the GAMA regions. The red line represents the homogeneous Metcalfe et al. (2001) LF prediction which at deep magnitudes is well normalized to the galaxy number counts. The points show the 2MASS (green circle) and GAMA (black cross) data with Poisson errors.

galaxies at $z \approx 0.1$ or large-scale inhomogeneities. Note that the above scale error correction tends to make the $K = 13.5$ galaxy counts ≈ 0.05 mag brighter, slightly improving the fit to the homogeneous model. The generally improved agreement between the LSS-corrected model and observed counts argues that the steep number count slopes are not caused by systematics in the magnitudes or in star–galaxy separation.

However, in all three regions the number counts are only becoming consistent with homogeneity at the $K = 13.5$ 2MASS limit, rather than the $K = 12.5$ limit we used for the $n(z)$. This leaves the possibility open that the underdensity may extend beyond the scales we have used in our LSS corrections and that the local volume remains underdense beyond ≈ 150–$300 \, h^{-1}$ Mpc. We interpret the consistency between $n(m)$ and $n(z)$ as evidence for a local hole-like underdensity at least out to $z \approx 0.08$.

6.2 Deeper *K* counts from GAMA

We next use the GAMA survey over the full $3 \times 48 \, \mathrm{deg}^2$ regions surveyed by the GAMA project to test the overall normalization of the homogeneous models for $n(z)$ and $n(m)$. We first calibrate the GAMA *K* Kron magnitudes to the 2MASS *K* k_m_ext magnitude scale by comparing the galaxy photometry. Using the 'mpfitexy' routine we find that all three GAMA regions are consistent with a one-to-one relation at $\approx 1\sigma$ as shown in Fig. A3. However, again using the 'mpfitexy' routine we find and apply the ≈ -0.02 mag zero-point offsets detailed in Table A1. We therefore compare the GAMA *K* counts and the three GAMA fields of 2MASS galaxy counts to the homogeneous models of Metcalfe et al. (2001) in Fig. 6. We see that the model fits the data well in the range $14 < K < 15.5$, supporting the normalization we have used from Table 1. We conclude that the normalization we have used is reinforced by the deeper *K* galaxy counts in the $150 \, \mathrm{deg}^2$ of the GAMA region.

7 *N*(*z*) TO *K* = 13.5 AND *r* = 17.2 IN THE SDSS-NGC REGION

It is possible to go to deeper *z*-survey limits in the SDSS-NGC region because of the fainter magnitude limit in this region, compared to 6dFGS. Figs 7 and 8 show the $n(z)$ and $\phi^*(z)$ for this region to the $K = 13.5$ limit of 2MASS. We normalize the $n(z)$ by the 96 per cent ratio of data-model number magnitude counts in this region to this limit – see Table 4. We note that the same basic features in $n(z)$ are seen at low redshift but new over- and underdensities appear at higher redshift. We note particularly the peak at $z \approx 0.08$. We see that it takes to $z \approx 0.13$ before the model fits the data. Indeed, the *K*-band counts in Fig. 4(c) only appear to converge at $K = 13.5$. We checked the difference that a no-evolution model made to the $n(z)$ fit and it was small. The no-evolution $n(K)$ model is also little different from the evolutionary model. The advantage of the *K* band is that it is less susceptible to evolutionary uncertainties.

Nevertheless, we also present the full $n(z)$ to $r = 17.2$ in the SDSS-NGC region. Here the $n(z)$ results are slightly more ambiguous. The $n(z)$ evolutionary model is compared to the data in Figs 9 and 10. The normalization factor to $r < 17.2$ from the $n(r)$ is 0.96 ± 0.02. The $r < 17.2 \, \phi(z)$ again shows evidence for underdensity but here the observed $\phi^*(z)$ generally is flatter, decreasing more slowly towards $z = 0$ than in *K*. Also it shows less indication of convergence at $z \approx 0.1$.

Clearly, the normalizing factor inferred from the *r*-band count is crucial here and we show $n(r)$ to $r < 22$ for the SDSS-NGC region in Figs 11 and 12. These counts are consistent with the Yasuda et al. (2001) analysis of the SDSS commissioning data for the magnitude range $15 < r < 20$. A similar behaviour is seen in Fig. 12 as in Fig. 10 in that the observed $n(r)$ takes till $r \approx 20$ to reach the homogeneous model. This is reinforced by the approximate agreement of the counts with the LSS-corrected model based on the $r < 17.2 \, n(z)$. Thus, there is at least consistency between the suggestions from $n(z)$ and $n(m)$ for the underdensity extending beyond $z = 0.1$.

Furthermore, there is uncertainty caused by the increased possibility of evolution in the *r* band. A no-evolution model for $n(m)$ is therefore also shown in Fig. 11. This model has a flatter slope and therefore reaches agreement with $n(r)$ at a brighter $r = 19$ magnitude. Thus here there would both be stronger evidence for a void within say $150 \, h^{-1}$ Mpc but the evidence for a more extended underdensity would be less than with the evolutionary model. It should also be noted that within the classes of models considered here, an evolutionary model gives a better fit to $n(r)$ at $r > 20$.

Uncertainties in the count normalization and the evolutionary model thus appear to be more significant in the *r* band, and this reinforces the advantage of working in *K*. The *K*-band counts may also be more sensitive to over- and underdensities, being more dominated by strongly clustered early-type galaxies. We conclude that the evidence in the *K* band for a local hole out to $300 \, h^{-1}$ Mpc can be regarded as more reliable than the more ambiguous evidence for a flatter underdensity to greater distances from the $r < 17.2 \, n(z)$.

8 THE HUBBLE DIAGRAM

Fig. 13 shows $\overline{z}(m)$ for our three fields. The homogeneous prediction for each region is shown as the red line and the LSS-corrected model, based on the $\phi^*(z)$ found earlier, is shown as the green line. In all three cases, we see that the green line gives an improved, although not perfect, fit to the data. But the importance of the LSS correction is clear since the underprediction of the observed $\overline{z}(m)$ particularly in the 6dFGS-SGC region might otherwise
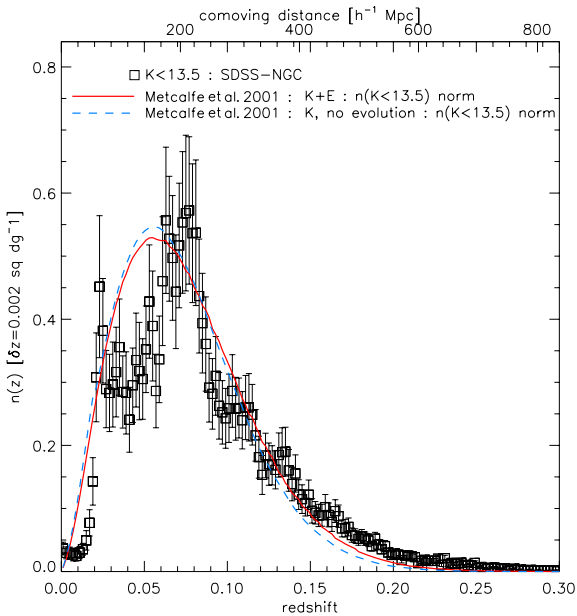
Figure 7. *K*-band galaxy $n(z)$ with $K < 13.5$ and $\delta z = 0.002$ normalized using the $K < 13.5$ galaxy number counts. The red line represents the homogeneous Metcalfe et al. (2001) LF prediction The points (black square) show the SDSS-NGC data with jack-knife derived errors.
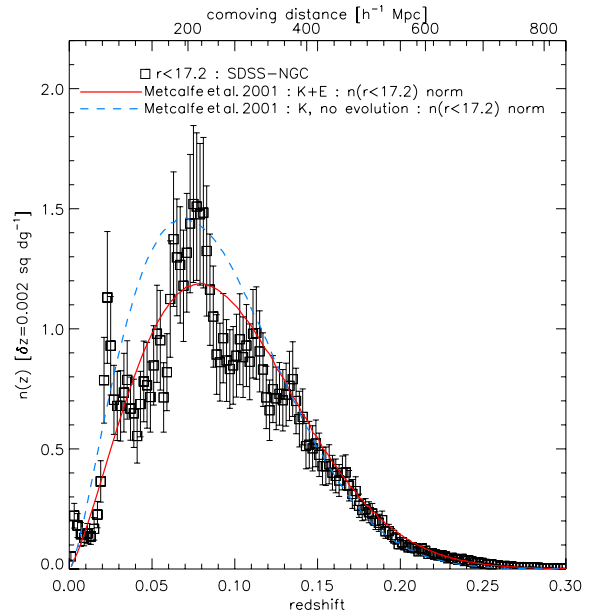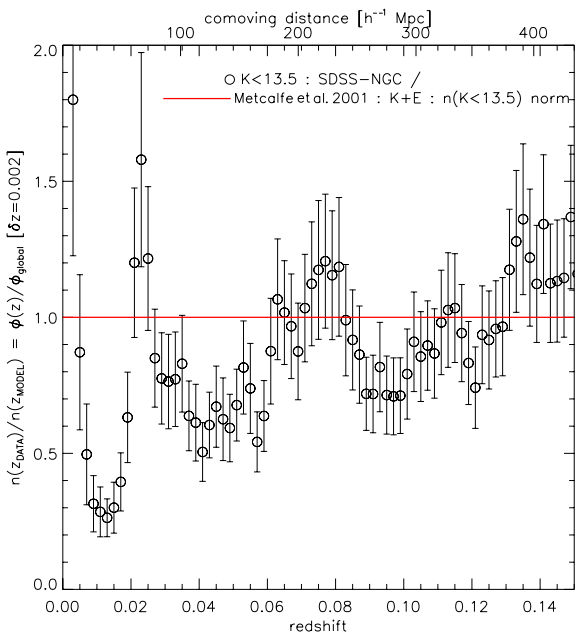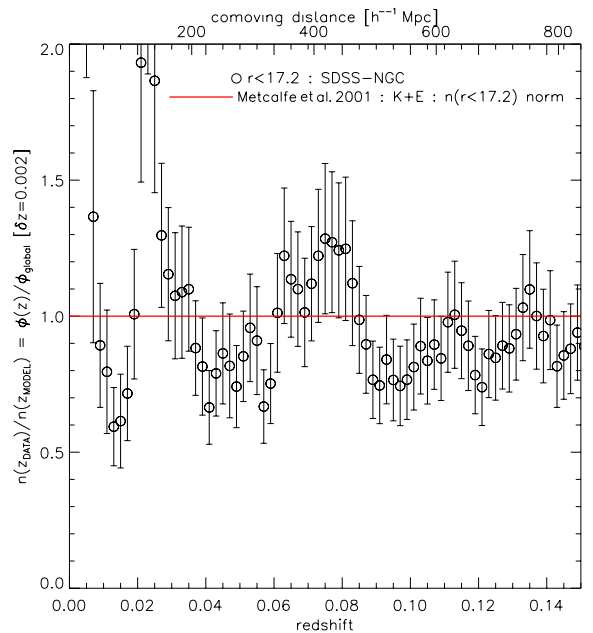

Figure 9. *r*-band galaxy $n(z)$ with $r < 17.2$ and $\delta z = 0.002$ normalized using the $r < 17.2$ galaxy number counts. The red line represents the homogeneous Metcalfe et al. (2001) LF prediction. The points (black square) show the SDSS-NGC data with jack-knife derived errors.

Figure 8. *K*-band galaxy $\phi^*(z)/\phi_{\mathrm{global}}$ with $K < 13.5$ and $\delta z = 0.002$ normalized using the $K < 13.5$ galaxy number counts. The red line represents the homogeneous Metcalfe et al. (2001) LF prediction. The points (black circle) show the SDSS-NGC data with jack-knife derived errors.

Figure 10. *r*-band galaxy $\phi^*(z)/\phi_{\mathrm{global}}$ with $r < 17.2$ and $\delta z = 0.002$ normalized using the $r < 17.2$ galaxy number counts. The red line represents the homogeneous Metcalfe et al. (2001) LF prediction. The points (black circle) show the SDSS-NGC data with jack-knife derived errors.

be interpreted as immediately implying peculiar motion which is clearly not the case. As expected, the 6dFGS-SGC region shows the biggest LSS (red–green) correction between the three regions since it showed the biggest low-redshift underdensity in Fig. 3 but the other two regions also tend to behave similarly. We also note the tentative 'spike' in $\overline{z}(m)$ in the 6dFGS-NGC region at $K \approx 11.5$, which is the approximate location of the Shapley-8 supercluster.

But even with $\delta m = 0.1$ mag bins, this technique does not have the resolution to detect backside infall.

To examine these $\overline{z}(m)$ relations in more detail, we next subtract the LSS-corrected 'Hubble law' prediction from the data in Fig. 13. This means we are in effect plotting a sky-averaged v_{pec}. The results are shown in Fig. 14 for a magnitude bin of $\delta m = 0.5$. For comparison, we also show the $\overline{z}(m)$ for the final $K = 12.25$ bin when using the original 2MASS 'k_m_ext' magnitude and without the
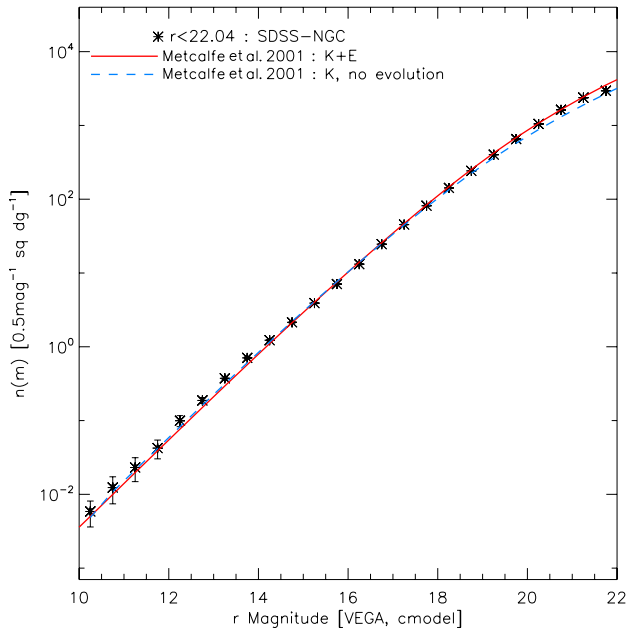
Figure 11. r-band galaxy $n(m)$ with $\delta m = 0.5$. The red line represents the homogeneous Metcalfe et al. (2001) LF prediction and the blue line the no-evolution homogeneous Metcalfe et al. (2001) LF prediction. The points (black asterisk) show the SDSS-NGC data with jack-knife derived errors.

Figure 12. r-band $n(m)$ based density contrast with $\delta m = 0.5$. The red line represents the homogeneous Metcalfe et al. (2001) LF prediction and the green line the LSS-corrected Metcalfe et al. (2001) LF prediction. The points (black asterisk) show the SDSS-NGC data with jack-knife derived errors.

spectroscopic completeness corrections described in Appendix B. The difference between these results means we cannot place too much weight on this final bin when interpreting these data. However, we note that over the rest of the magnitude range this difference is small, particularly so for the 6dFGS-NGC/SGC fields. We therefore conclude that completeness corrections are only important for the final magnitude bin and the SDSS-NGC data.

Since the models indicated by the green lines assume that galaxies are at rest in the Local Group frame, then this is tantamount to assuming that all galaxies and the Local Group are moving with a coherent bulk notion. We now investigate an alternative hypothesis that the Local Group is moving with 633 km s^{-1} relative to more distant galaxies, i.e. the CMB dipole motion in the Local Group frame. The relative average recession velocity of these distant galaxies should then be correspondingly reduced in the direction of our motion relative to the CMB and increased in the opposite direction. This 'dipole' non-bulk motion model is then represented by the blue lines in Fig. 14.

We immediately see that in two out of three regions, the bulk motion prediction agrees with the data much better than the non-bulk motion model where only the Local Group is moving with 633 km s^{-1} with respect to the CMB. Even in the third region in the 6dFGS-SGC direction, although the data agree better with the non-bulk motion model, it is also still in reasonable agreement with the bulk motion model. The significance of the rejection of the non-bulk motion model has been estimated using the $K = 11.75$ bin. This is necessary as the smoothing by the galaxy LF causes different magnitude bins to be highly covariant and also the final bin may be less reliable as discussed above. The level of rejection of the non-bulk motion model in the 6dFGS-NGC and SDSS-NGC regions is at the 3.1σ and 2.3σ levels, respectively. This suggests that at least in the 6dFGS-NGC and SDSS-NGC directions, we may be seeing a bulk motion with convergence to the CMB dipole not yet reached at our $K < 12.5$ mag survey limits. Combining the measurements across all three regions, we find an overall rejection of the non-bulk
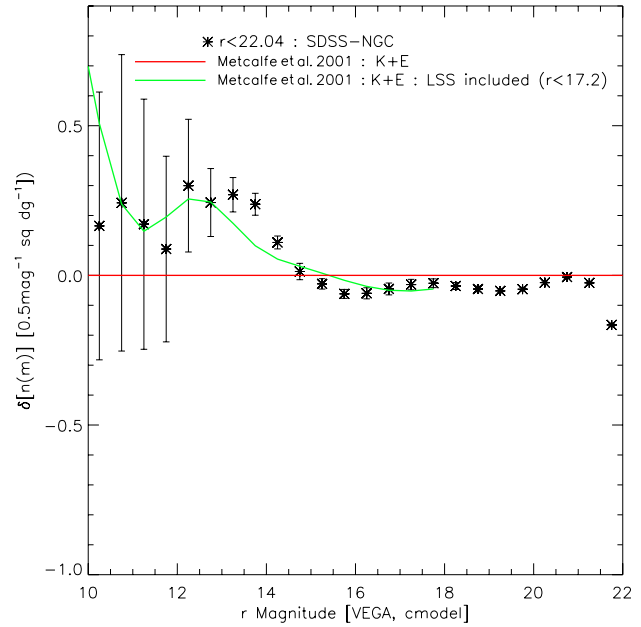
motion model at the 3.9σ level. In contrast, the bulk motion model is consistent with the data overall at the 1.5σ level. The fit of the bulk motion model indicates that the scale of convergence is larger than the $\approx$150 h^{-1} Mpc scale probed at $K < 12.5$. However, it should be noted that the residual dipole effect is small relative to the LSS correction.

It is somewhat counter-intuitive that the regions which are less underdense on average (6dFGS-NGC, SDSS-NGC) agree with the bulk motion model whilst the most underdense region (6dFGS-SGC) agrees with the dipole-based non-bulk motion model. However, this might be consistent with a faster local expansion in the most underdense area. In this view, the agreement of 6dFGS-SGC $\bar{z}(m)$ with the non-bulk motion model (blue line) would be accidental with the real interpretation being a bulk motion (green line) combined with a faster local expansion resulting in an excess v_{pec} as is observed. We note that in the other two regions, there is at least no inconsistency with a faster local expansion rate relative to the bulk motion model. But it should still be noted that our simple models do not include peculiar velocities generated by structures like Shapley-8 in 6dFGS-NGC which would produce apparently higher expansion rates even beyond their nominal redshift, due to the smoothing of $\bar{z}(m)$ by the galaxy LF. Similarly, these models may be somewhat affected by an inhomogeneous Malmquist bias from LSS at deeper redshifts that is not fully accounted for with our $K < 12.5$ derived $\phi(z)$ density profiles.

We conclude that the successful fit of a bulk motion model fit to $\bar{z}(m)$ may be consistent with the $\approx$150 h^{-1} Mpc scale coherent underdensity found in $n(z)$ and $n(m)$ across our three regions. The question of whether the 300 h^{-1} Mpc void is visible dynamically in $\bar{z}(m)$ is less clear because that statistic does not reach $z \approx 0.1$. Clearly, the SNIa Hubble diagram probes out to larger redshifts where it is a more probable standard candle than our galaxy samples. The question then of whether there is dynamical evidence of a local hole is of course intertwined with the cosmological model that is assumed.
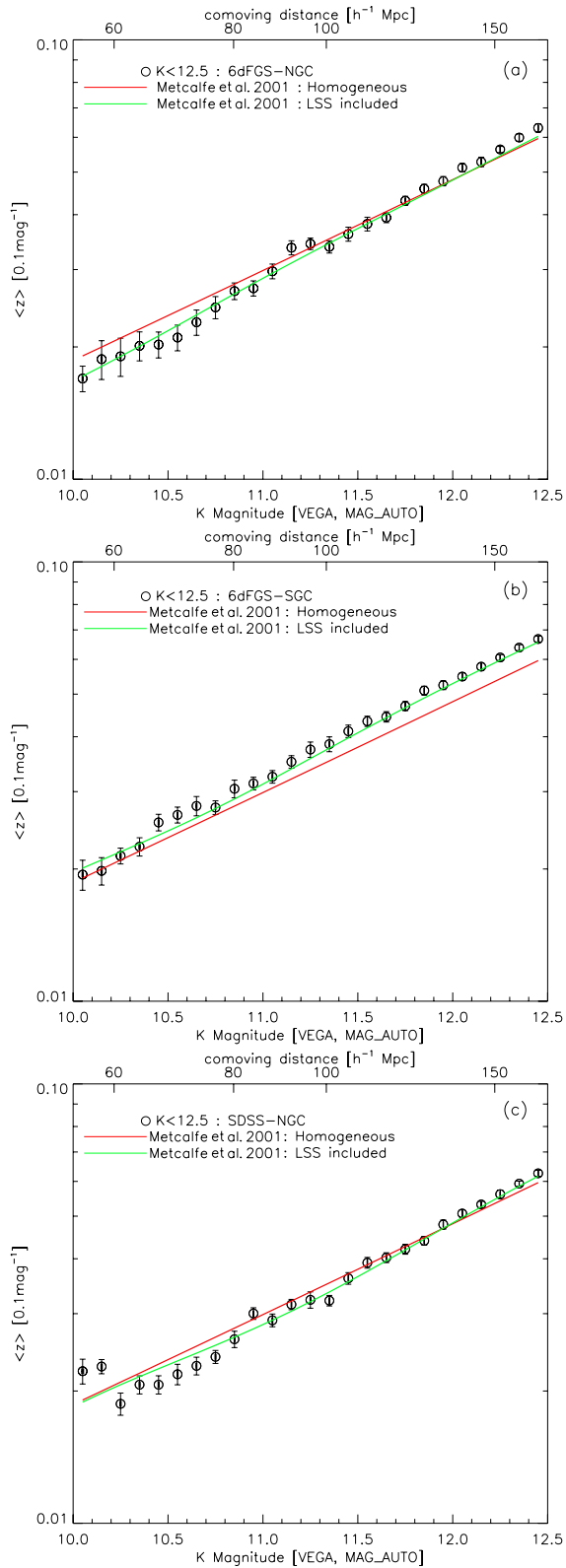
Figure 13. *K*-band $\bar{z}(m)$ with $\delta m = 0.1$. The red line represents the homogeneous Metcalfe et al. (2001) LF prediction and the green line the LSS-corrected Metcalfe et al. (2001) LF prediction. The points (black circle) show data with jack-knife derived errors. (a) 6dFGS-NGC region (6dFGS, galactic north), (b) 6dFGS-SGC region (6dFGS, galactic south), (c) SDSS-NGC (SDSS-2MASS, galactic north).
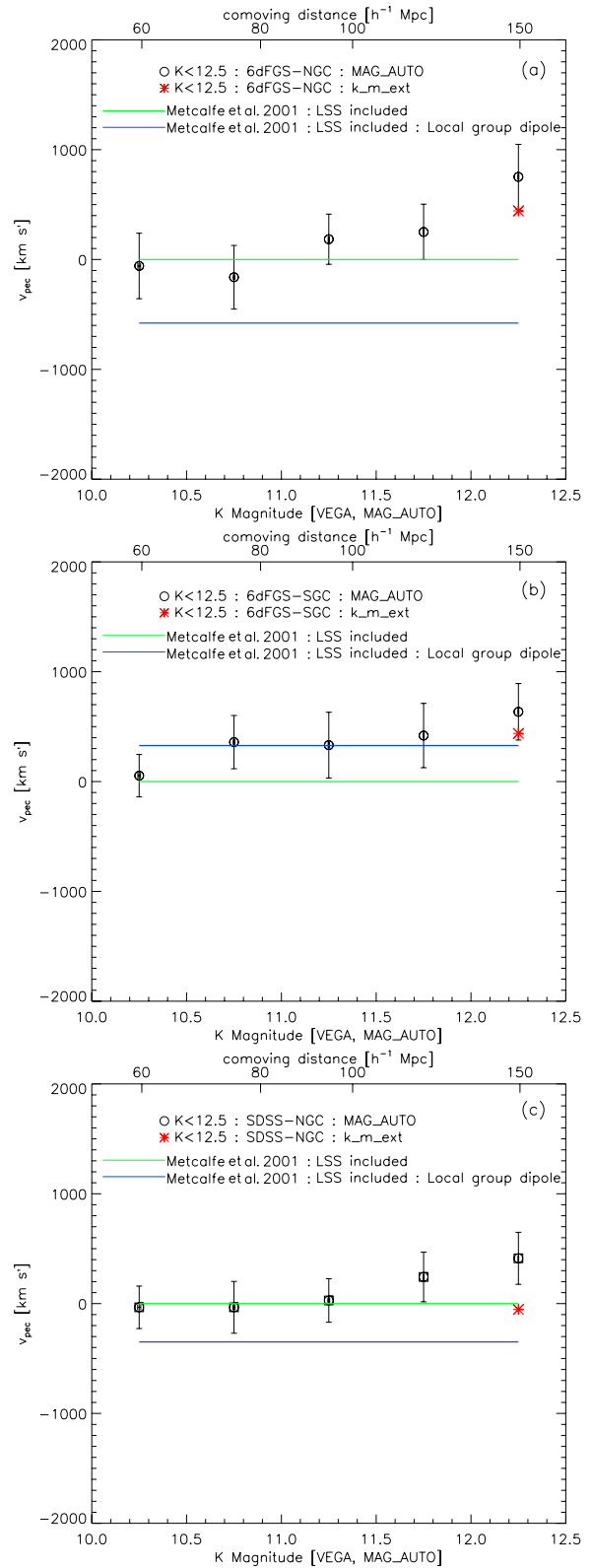
Figure 14. *K*-band $\bar{z}(m)$ with $\delta m = 0.5$. The green line represents the LSS-corrected Metcalfe et al. (2001) LF prediction and the blue line the CMB dipole flow LSS-corrected Metcalfe et al. (2001) LF prediction. The points (black circle) show data with jack-knife derived errors. The red asterisk shows the final bin without corrections. (a) 6dFGS-NGC region (6dFGS, galactic north), (b) 6dFGS-SGC region (6dFGS, galactic south), (c) SDSS-NGC (SDSS-2MASS, galactic north).

9 CONCLUSIONS

We have used $n(m)$ from 2MASS and $n(z)$ from 6dFGS and SDSS limited at $K < 12.5$ over much of the sky at high galactic latitudes to probe the local LSS, extending the work of Frith et al. (2005b). We looked at three volumes and found that that in the 6dFGS-SGC region, which broadly corresponds to the area previously covered by the APM survey, there is a clear ≈ 40 per cent underdensity out to $150\, h^{-1}$ Mpc. In the SDSS-NGC volume, an ≈ 15 per cent underdensity is seen again out to $150\, h^{-1}$ Mpc, although this is broken by the Coma cluster producing a strong overdensity at $\approx 75\, h^{-1}$ Mpc in front of large underdensities behind it. An ≈ 5 per cent underdensity is seen in the 6dFGS-NGC area out to about $150\, h^{-1}$ Mpc. The implied local underdensity in $n(z)$ and $n(m)$ averaged over the three fields out to $K < 12.5$ is $\approx 15 \pm 3$ per cent. Modelling the K number counts using the ratio of a homogeneous model normalized to these over- and underdensities to define $\phi^*(z)$ produced good agreement with the underdensities seen in the number counts to $K = 12.5$, particularly in the 6dFGS-SGC area. This agreement between $n(m)$ and $n(z)$ supports the reality of these local inhomogeneities out to $\approx 150\, h^{-1}$ Mpc depth.

While ΛCDM may allow structures on 200–$300\, h^{-1}$ Mpc scales (Yadav, Bagla & Khandai 2010; Park et al. 2012; Watson et al. 2013), Frith et al. (2005b) calculated that a 24 per cent underdensity to $K < 12.5$ over the 4000 deg^2 APM (6dFGS-SGC) area would be inconsistent with the ΛCDM model at the 4–4.5σ level, depending on whether the calculation was based on a theoretical ΛCDM or observed 2MASS $w(\theta)$ – see their table 1. However, when these authors take into account the previous uncertainties in the K-band count normalization, this significance then reduced to 2–3σ. Here, we have confirmed the 6dFGS-SGC underdensity to be 24 ± 3 per cent at $K < 12.5$ in only a slightly smaller area (3511 deg^2) and further confirmed that our number count normalization is accurate from the deeper GAMA data, in an area ≈ 600 times larger than that available to Frith et al. (2005b). So the existence of such a coherent underdensity in the south Galactic cap appears to imply an $\approx 4\sigma$ discrepancy with the ΛCDM model, in terms of the large-scale power that it predicts.

The use of the LF of Metcalfe et al. (2001) is a potential area of weakness in these studies. However, Shanks & Whitbourn (in preparation) use ML techniques to estimate the LF and $\phi^*(z)$ simultaneously for the r- and K-limited samples. They find that our assumed LF is either in good agreement with the self-consistently estimated LF (r band) or where it differs slightly (K band) the $\phi^*(z)$ results prove robust and unaffected.

We then made a Hubble diagram using the $\bar{z}(m)$ technique of Soneira (1979). Before we could detect peculiar velocities, we had to make LSS corrections to make the model for $\bar{z}(m)$ take account of the inhomogeneities already found. In the 6dFGS-SGC region, we found that the LSS-corrected $\bar{z}(m)$ prefers a solution that includes a $633\ \mathrm{km\,s^{-1}}$ CMB velocity component for the Local Group relative to galaxies in this direction. In the 6dFGS-NGC and SDSS-NGC regions, the more distant galaxies still preferred the solution without the CMB velocity added to the Local Group and so can be said to prefer a bulk motion solution where the local motion towards the CMB dipole direction has not converged.

The local underdensities we have found will imply faster local expansions. Indeed, we noted that such a scenario is not inconsistent with the results we found with $\bar{z}(m)$. Such a faster local expansion could help alleviate the tension at the ≈ 5 per cent level between recent local and CMB measures of H_0 [Ade P. A. R. et al. (Planck Collaboration) 2013]. The naive expectation for the effect on H_0 can be derived by assuming linear theory, $\delta H_0/H_0 = -\frac{1}{3}\Omega_m^{0.6}/b \times \delta\rho_g/\rho_g$, where the bias $b \approx 1$ for the standard model. Then the 19 ± 3 per cent, $z < 0.05$, $K < 12.5$, underdensity we report suggests an ≈ 2–3 per cent increase in H_0. Indeed, this level of variation is not inconsistent with estimates of the cosmic variance of H_0 in ΛCDM (Kalus et al. 2013; Marra et al. 2013). However, for the southern Galactic cap region where we found a deeper underdensity of ≈ 40 per cent, a larger H_0-correction of 6–7 per cent would be implied.

Finally, we investigated the evidence for an even larger local underdensity out to $\approx 300\, h^{-1}$ Mpc. We first determined the $n(m)$ normalization at fainter $K \approx 16$ mag and $r \approx 20.5$ mag from GAMA and SDSS. We found excellent agreement with the K model counts at $K \approx 15$. This normalization implies that the underdensity in the SDSS-NGC volume may extend to $\approx 300\, h^{-1}$ Mpc and even deeper if the SDSS-NGC $r < 17.2\ n(z)$ is to be believed. However, there is increased uncertainty in r due to the likelihood of increased evolutionary effects as well as the count model normalization uncertainty. Although $\bar{z}(m)$ at these limits cannot test further this $300\, h^{-1}$ Mpc underdensity dynamically, we have noted that any cosmology that fits the SNIa Hubble diagram before accounting for the local hole must fail at some level afterwards.

ASKAP providing UV to radio coverage. GAMA is funded by the STFC (UK), the ARC (Australia), the AAO and the participating institutions. The GAMA website is http://www.gama-survey.org/.

This research has made use of the NASA/IPAC Extragalactic Database (NED) which is operated by the Jet Propulsion Laboratory, California Institute of Technology, under contract with the National Aeronautics and Space Administration. This research has also made use of the VizieR catalogue access tool, CDS, Strasbourg, France. The original description of the VizieR service was published in A&AS 143, 23 (2000). We have made use of the mpfitexy routine (Williams, Bureau & Cappellari 2010). The mpfitexy routine depends on the MPFIT package (Markwardt 2009). We would also like to acknowledge the use of the TOPCAT utility.

REFERENCES

Abate A., Feldman H. A., 2012, MNRAS, 419, 3482
Ade P. A. R., et al. (Planck Collaboration), 2013, preprint (arXiv:1303.5076)
Ahn C. P. et al., 2012, ApJS, 203, 21
Barro G. et al., 2009, A&A, 494, 63
Bell E. F., McIntosh D. H., Katz N., Weinberg M. D., 2003, ApJS, 149, 289
Bilicki M., Chodorowski M., Jarrett T., Mamon G. A., 2011, ApJ, 741, 31
Biswas T., Notari A., Valkenburg W., 2010, J. Cosmol. Astropart. Phys., 11, 30
Blake C., Wall J., 2002, Nature, 416, 150
Blanton M. R., Roweis S., 2007, AJ, 133, 734
Branchini E., Davis M., Nusser A., 2012, MNRAS, 424, 472
Bruzual G., Charlot S., 2003, MNRAS, 344, 1000
Busswell G. S., Shanks T., Frith W. J., Outram P. J., Metcalfe N., Fong R., 2004, MNRAS, 354, 991
Célérier M. N., Thieberger R., 2005, in Chen P., Bloom E., Madejski G., Patrosian V., eds, Proc. 22nd Texas Symp. on Relativistic Astrophysics: Fractal Dimensions of the Galaxy Distribution Varying by Steps? p. 364, available at: http://www.slac.stanford.edu/econf/C041213/proceedings.html
Chodorowski M. J., Coiffard J., Bilicki M., Colombi S., Ciecielag P., 2008, MNRAS, 389, 717
Cole S. et al., 2001, MNRAS, 326, 255
Colin J., Mohayaee R., Sarkar S., Shafieloo A., 2011, MNRAS, 414, 264
Colless M. et al., 2001, MNRAS, 328, 1039
Cross N. et al., 2001, MNRAS, 324, 825
Driver S. P., Windhorst R. A., Ostrander E. J., Keel W. C., Griffiths R. E., Ratnatunga K. U., 1995, ApJ, 449, L23
Driver S. P. et al., 2009, Astron. Geophys., 50, 050000
Driver S. P. et al., 2011, MNRAS, 413, 971
Erdoğdu P. et al., 2006, MNRAS, 368, 1515
February S., Larena J., Smith M., Clarkson C., 2010, MNRAS, 405, 2231
Feldman H. A., Watkins R., Hudson M. J., 2010, MNRAS, 407, 2328
Finlator K. et al., 2000, AJ, 120, 2615
Frith W. J., Busswell G. S., Fong R., Metcalfe N., Shanks T., 2003, MNRAS, 345, 1049
Frith W. J., Outram P. J., Shanks T., 2005a, in Fairall K. P., Woudt P. A., eds, ASP Conf. Ser. Vol. 329, Nearby Large-Scale Structures and the Zone of Avoidance. Astron. Soc. Pac., San Francisco, p. 49
Frith W. J., Shanks T., Outram P. J., 2005b, MNRAS, 361, 701
Frith W. J., Metcalfe N., Shanks T., 2006, MNRAS, 371, 1601
Gibelyou C., Huterer D., 2012, MNRAS, 427, 1994
Glazebrook K., Ellis R., Santiago B., Griffiths R., 1995, MNRAS, 275, L19
Gott J. R., III, Jurić M., Schlegel D., Hoyle F., Vogeley M., Tegmark M., Bahcall N., Brinkmann J., 2005, ApJ, 624, 463
Hill D. T. et al., 2011, MNRAS, 412, 765
Hogg D. W., Eisenstein D. J., Blanton M. R., Bahcall N. A., Brinkmann J., Gunn J. E., Schneider D. P., 2005, ApJ, 624, 54
Jarrett T. H., Chester T., Cutri R., Schneider S. E., Huchra J. P., 2003, AJ, 125, 525
Jones D. H. et al., 2004, MNRAS, 355, 747

Jones D. H. et al., 2009, MNRAS, 399, 683
Kalus B., Schwarz D. J., Seikel M., Wiegand A., 2013, A&A, 553, A56
Karachentsev I. D., Makarov D. A., 1996, AJ, 111, 794
Kashlinsky A., Atrio-Barandela F., Kocevski D., Ebeling H., 2008, ApJ, 686, L49
Keenan R. C., Trouille L., Barger A. J., Cowie L. L., Wang W., 2010, ApJS, 186, 94
Keenan R. C., Barger A. J., Cowie L. L., Wang W.-H., Wold I., Trouille L., 2012, ApJ, 754, 131
Keenan R. C., Barger A. J., Cowie L. L., 2013, ApJ, 775, 62
Keisler R., 2009, ApJ, 707, L42
Labini F. S., 2011, Class. Quantum Gravity, 28, 164003
Lavaux G., Afshordi N., Hudson M. J., 2013, MNRAS, 430, 1617
Liske J., Lemon D. J., Driver S. P., Cross N. J. G., Couch W. J., 2003, MNRAS, 344, 307
Loveday J., 2000, MNRAS, 312, 557
Maddox S. J., Efstathiou G., Sutherland W. J., Loveday J., 1990, MNRAS, 243, 692
Markwardt C. B., 2009, in Bohlender D. A., Durand D., Dowler P., eds, ASP Conf. Ser. Vol. 411, Astronomical Data Analysis Software and Systems XVIII. Astron. Soc. Pac., San Francisco, p. 251
Marra V., Amendola L., Sawicki I., Valkenburg W., 2013, Phys. Rev. Lett., 110, 241305
McIntosh D. H., Bell E. F., Weinberg M. D., Katz N., 2006, MNRAS, 373, 1321
Metcalfe N., Shanks T., Campos A., Fong R., Gardner J. P., 1996, Nature, 383, 236
Metcalfe N., Shanks T., Campos A., McCracken H. J., Fong R., 2001, MNRAS, 323, 795
Metcalfe N., Shanks T., Weilbacher P. M., McCracken H. J., Fong R., Thompson D., 2006, MNRAS, 370, 1257
Moss A., Zibin J. P., Scott D., 2011, Phys. Rev. D, 83, 103515
Murphy D. N. A., Eke V. R., Frenk C. S., 2011, MNRAS, 413, 2288
Nadathur S., Sarkar S., 2011, Phys. Rev. D, 83, 063506
Nusser A., Branchini E., Davis M., 2011, ApJ, 735, 77
Osborne S. J., Mak D. S. Y., Church S. E., Pierpaoli E., 2011, ApJ, 737, 98
Park C., Choi Y.-Y., Kim J., Gott J. R., III, Kim S. S., Kim K.-S., 2012, ApJ, 759, L7
Peebles P. J. E., Nusser A., 2010, Nature, 465, 565
Perlmutter S. et al., 1999, ApJ, 517, 565
Regis M., Clarkson C., 2012, Gen. Relativ. Gravitation, 44, 567
Rood H. J., 1988, ARA&A, 26, 245
Sarkar P., Yadav J., Pandey B., Bharadwaj S., 2009, MNRAS, 399, L128
Schechter P., 1976, ApJ, 203, 297
Schlegel D. J., Finkbeiner D. P., Davis M., 1998, ApJ, 500, 525
Schmidt B. P. et al., 1998, ApJ, 507, 46
Scrimgeour M. I. et al., 2012, MNRAS, 425, 116
Shanks T., Stevenson P. R. F., Fong R., MacGillivray H. T., 1984, MNRAS, 206, 767
Skrutskie M. F. et al., 2006, AJ, 131, 1163
Soneira R. M., 1979, ApJ, 230, L63
Strauss M. A. et al., 2002, AJ, 124, 1810
Watkins R., Feldman H. A., Hudson M. J., 2009, MNRAS, 392, 743
Watson W. A., Iliev I. T., Diego J. M., Gottlöber S., Knebe A., Martínez-González E., Yepes G., 2013, preprint (arXiv:1305.1976)
Williams M. J., Bureau M., Cappellari M., 2010, MNRAS, 409, 1330
Yadav J. K., Bagla J. S., Khandai N., 2010, MNRAS, 405, 2009
Yasuda N. et al., 2001, AJ, 122, 1104
York D. G. et al., 2000, AJ, 120, 1579

APPENDIX A: MAGNITUDE ACCURACY

A1 2MASS k_m_ext

Here we aim to test for scale and zero-point errors in our 2MASS k_m_ext magnitudes. We therefore compare to the previous galaxy photometry of Loveday (2000) where pseudo-total MAG_BEST

Table A1. A summary of the zero-point corrections applied to the GAMA data to calibrate on to the 2MASS photometric scale as derived using the 'mpfitexy' routine when assuming no scale error.

Field	Number	$K_{2MASS} - K_{GAMA}$
G09	567	(-0.02 ± 0.01)
G12	750	(-0.03 ± 0.01)
G15	725	(-0.02 ± 0.01)
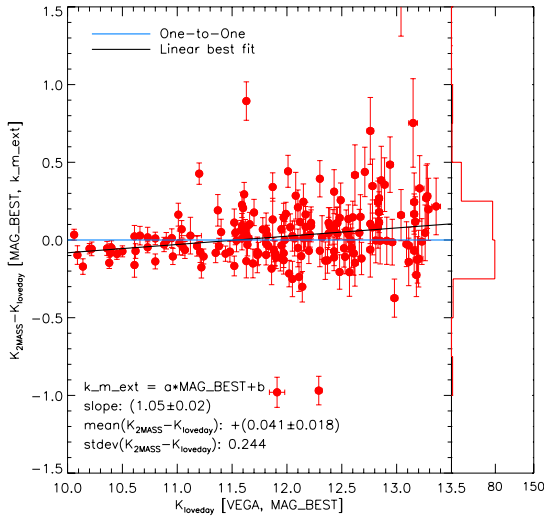
Figure A1. *K*-band magnitude comparison for 181 common galaxies of the deep *K* data of Loveday (2000) who have provided the *MAG_BEST* magnitude from SExtractor to the corresponding 2MASS k_m_ext magnitude. The derived slope using the 'mpfitexy' routine and both the mean and standard deviation of the residuals are stated.

magnitudes were measured using SExtractor. In Fig. A1, we show the resulting comparison after matching the Loveday (2000) galaxies to 2MASS with a 3 arcsec matching radius.

First, assuming no scale error we find a marginally significant zero-point offset of k_m_ext-MAG_BEST $= 0.04 \pm 0.02$ mag. Then we test for non-linearity by fitting for a scale error using the 'mpfitexy' routine considering errors in both magnitudes. We find a slope of k_m_ext $= (1.05 \pm 0.02)$MAG_BEST. Whilst this is only significant at the $\approx 2\sigma$ level, we nevertheless applied this correction factor to the k_m_ext magnitude thereby placing the 2MASS data on the Loveday (2000) system. Although this has the effect of slightly steepening the 2MASS counts in Fig. 4, the effect on the overall conclusions is negligible.

We further check the 2MASS k_m_ext magnitude by comparing to the 2MASS Kron magnitude (k_m_e) for the Loveday (2000) galaxies in Fig. A2. Both these 2MASS magnitudes are pseudo-total so a one-to-one relationship might be expected. First we find a simple offset of k_m_ext-Kron $= -0.05 \pm 0.01$ mag. Although this is significant, for this work offsets are less important than scale errors. We test for such a scale error as above and find a slope of k_m_ext $= (1.02 \pm 0.01)$Kron; thus, the k_m_ext and Kron magnitudes seem reasonably consistent with a one-to-one relation.

We note that in Fig. 6 we have not corrected the 2MASS+GAMA magnitudes on to the Loveday (2000) system. This is conservative since the effect would be to imply a slightly higher (≈ 3 per cent) normalization for our Metcalfe et al. (2001) LF and homogeneous count model.
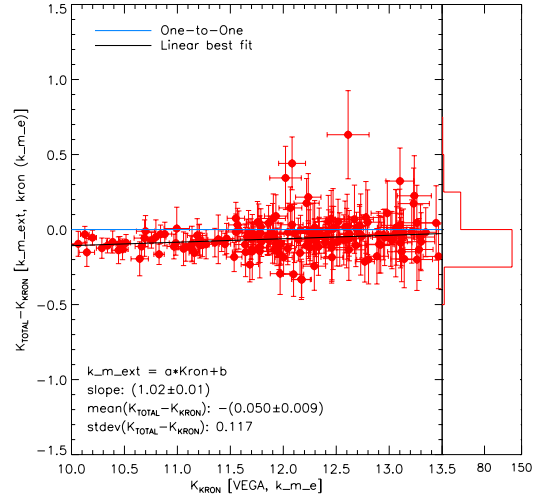

Figure A2. An internal *K*-band magnitude comparison of the 2MASS k_m_ext and the elliptical Kron (k_m_e) magnitudes for 181 common galaxies of the deep *K* data of Loveday (2000). The derived slope using the 'mpfitexy' routine and both the mean and standard deviation of the residuals are stated.
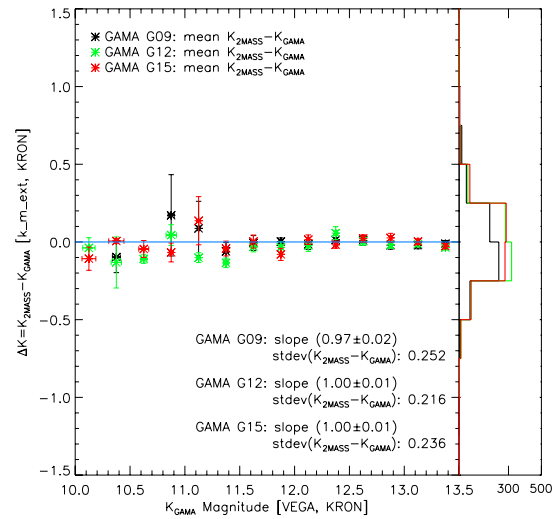

Figure A3. *K*-band magnitude comparison between GAMA Kron and 2MASS k_m_ext magnitudes over the GAMA regions. The derived slope using the 'mpfitexy' routine and the standard deviation of the residuals are stated.

A2 SDSS cmodel

We now test the SDSS cmodel magnitude using Kron magnitudes from the extended William Herschel Deep Field (WHDF) region Cousins *R*-band data of Metcalfe et al. (2001, 2006). Although some non-linearity is seen in Fig. A4, this is due to saturation of the WHDF bright magnitudes. In the range $17 < r < 22$, visually there seems little evidence of a scale error and this is confirmed by an analysis using 'mpfitexy' where we find a slope of $r_{cmodel} = (1.02 \pm 0.01)R_{WHDF}$. If we then assume no scale error, we find a simple zero-point offset of $r_{cmodel} - R_{WHDF} = (0.07 \pm 0.01)$mag. However, for the SDSS *r*-band count in Fig. 12, we have in fact assumed the larger offset of $r_{cmodel} - R_{WHDF} = 0.12$mag to ensure that the counts at $r > 21$ are in agreement with the homogeneous model as might be expected at this depth.
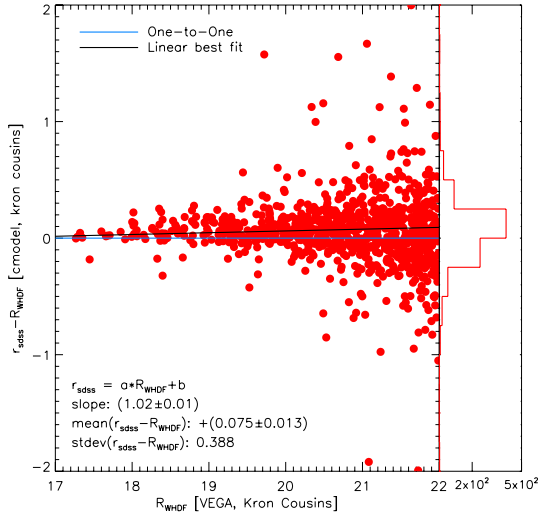
Figure A4. Magnitude comparison between WHDF Kron Cousins *R* and SDSS cmodel *r* over the extended WHDF region. The derived slope using the 'mpfitexy' routine and both the mean and standard deviation of the residuals are stated.

APPENDIX B: INCOMPLETENESS EFFECTS

B1 Photometric incompleteness

B1.1 2MASS

2MASS is ≈ 97.5 per cent complete to $K < 13.57$ as described at http://www.ipac.caltech.edu/2mass/releases/allsky/doc/sec6_1k.html. Star–galaxy separation for $|b| > 20°$ has been determined by eye to be >99 per cent reliable to at least $K < 12.8$ and only falling to 97 per cent by $K = 13.5$ as outlined at http://www.ipac.caltech.edu/2mass/releases/allsky/doc/sec6_5b2.html.

B1.2 SDSS

The SDSS *r*-band photometric catalogue is magnitude limited to $r < 22.04$ and has been validated by comparison to COMBO-17 as discussed at http://www.sdss3.org/dr9/imaging/other_info.php#completeness. Any significant incompleteness is only present at magnitudes $r > 21$ which is far fainter than the scales relevant for studying a local $300\ h^{-1}$ Mpc underdensity.

Equally, SDSS has studied the validity of its star–galaxy separation relative to COMBO-17 at http://www.sdss3.org/dr9/imaging/other_info.php#stargalaxy. Significant issues in classification arise at bright magnitudes $r < 15$ and at faint magnitudes $r > 20$. Only the problem at the bright end is relevant for interpreting the number counts at the local hole scales. However, the agreement between the spectroscopically derived $\phi^*(z)$ models and the photometric number counts suggests that star–galaxy separation is not biasing the bright-end results.

B2 Spectroscopic incompleteness

In Figs B2 and B1, we show, respectively, the spectroscopic incompleteness of the *K* and *r* samples used in this paper. Also reported are the ratios of the total number of spectroscopic to photometric galaxies for each sample. We can see that the incompleteness increases for brighter galaxies, particularly in the case of the *r*- and *K*-band SDSS-NGC samples. This is caused by the relative importance of
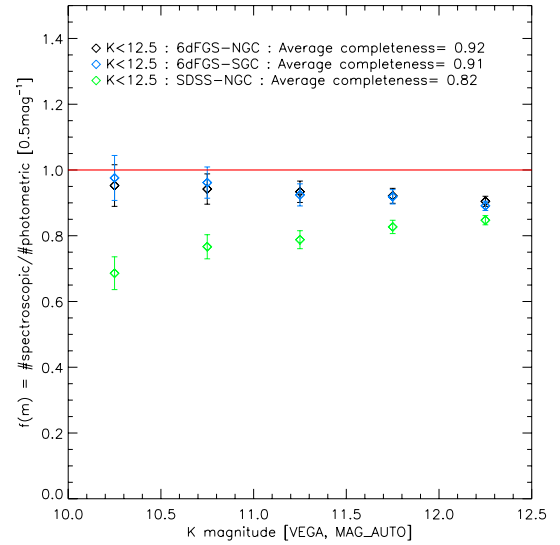

Figure B1. *K*-band spectroscopic incompleteness as a function of magnitude as derived from the ratio of spectroscopic (6dFGS and SDSS) to photometric (2MASS) number counts with $\delta m = 0.1$. Poisson errors are shown.
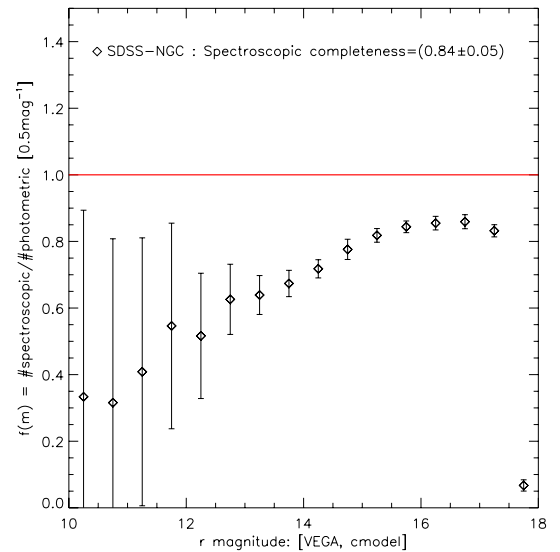

Figure B2. *r*-band spectroscopic incompleteness as a function of magnitude as derived from the ratio of spectroscopic (SDSS) to photometric (SDSS) number counts with $\delta m = 0.1$. Poisson errors are shown.

image artefacts and fibre constraints for large/bright galaxies in SDSS (Bell et al. 2003; McIntosh et al. 2006).

We first correct the number of galaxies in the data $n(z)$ to the same total as in the corresponding data $n(m)$ by multiplying the data $n(z)$ by the ratio of the total number of photometric to spectroscopic galaxies in each sample. Next, we account for the magnitude dependence of spectroscopic incompleteness in the model $n(z)$ as shown in Figs B1 and B2. We do this by introducing magnitude-dependent completeness factor $f(m)$ into the modelling procedure as in equation (1) by adjusting $\Phi(M)$ as follows:

$$\Phi(M) \equiv \Phi(m - 5\log d_L(z) - 25 - K(z) - E(z)),$$
$$\rightarrow f(m)\Phi(m - 5\log d_l(z) - 25 - K(z) - E(z)), \quad \text{(B1)}$$

while conserving galaxy numbers in the model $n(z)$. A similar technique was then applied to correct $\bar{z}(m)$.

Finally, even at the low-redshift end the change due to this procedure is less than 1 per cent in the $n(z)$ for both the K- and r-limited spectroscopic data sets. It is therefore irrelevant for interpreting the density profiles shown in Figs 3, 8 and 10. However, the effect is somewhat more appreciable in $\bar{z}(m)$, especially for the SDSS-NGC K sample where the completeness correction can cause bins to vary by as much as $100\ \mathrm{km\,s^{-1}}$. This is due to the stronger variations in spectroscopic incompleteness for this sample.

This paper has been typeset from a TEX/LATEX file prepared by the author.